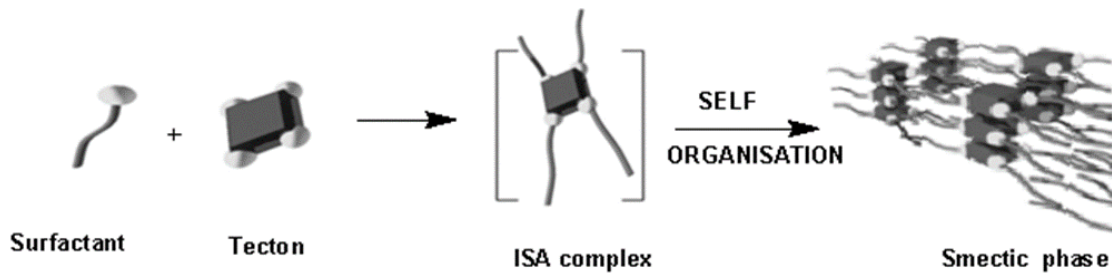


## Chapter-2

### *Synthesis and mesomorphism of discotic polyanion- surfactant complexes*

#### **Abstract**

*Disc-shaped systems have often been found to assemble in columnar structures. The polyelectrolyte surfactant complexes have been found to be having large scope in biological processes. In this current report, we have employed a discotic core as a polyanionic scaffold and complexed with double tail surfactants via the ionic self-assembly approach. The ionic self-assembled complexes have been found to have good thermal stability. The complexes were found to be mesomorphic in nature as a function of temperature. Further, they have been studied for self-assembly behavior in the aqueous medium. The complex –water system has been found to be exhibiting lamellar mesophase.*



## 2.1 Introduction

The construction of novel materials involves the interplay among molecular structure, intermolecular interactions, order, and macroscopic properties<sup>1</sup>. Non-covalent interactions play a vital role in the design of new materials. The advantage of inducing non-covalent interactions has gained large attention mainly due to their easier processability<sup>2</sup>. The non-covalent interactions have been found to be a vital factor in the development of high anisotropic and stable structures. The self-organization often leads to association into ordered aggregates as a result of the involvement of non-covalent interactions (**Table 2.1**). Non-covalent strategies involve H-bonding, metal coordination, charge assisted H-bonding, these strategies have been successfully employed to induce mesogenicity in the systems<sup>3</sup>. The main challenge involving these approaches revolves around the manipulation of structural and macroscopic order. The order in these systems depends on shape, chemical functionality, strength and direction of secondary interactions<sup>4</sup>.

Ionic self-assembly (ISA) is defined as the self-organization of tectonic units under the influence of coulombic interactions<sup>5</sup>. Further, the important factor which is associated with ISA is the cooperative binding mechanism. The cooperativity in self-organization is nothing but the first binding which stimulates further binding which further propagates self-assembled structures. Ionic self-assembly is contrary to salt association which is long-range and non-selective<sup>6</sup>. Further one of the hallmarks of ISA is that it makes use of tectonic units with diversity in shape, functionality, cohesion energy distribution along charged sites where secondary structural units induce alignment through the charge-charge coupling. Ionic self-assembly has been used in the formation of functional materials. The principle of ISA involves two oppositely charged tectons forming a charge neutralized supramolecular complex. This process is similar to polyelectrolyte – surfactant/lipid systems, where the assembly involves cooperativity. The properties of complexes formed due to the combination of charged tectons can be fine-tuned by the choice of tectons. Dye molecules on complexation with oppositely charged tectons result in gel formation with fibrillar morphology with high degree of order<sup>7</sup>.

Interaction	Strength(KJmol <sup>-1</sup> )	Range	Character
Van der Waals	~ 50	Short	non-selective Non-directional
H-bonding	5-65	Short	Selective Directional
Coordination	50-200	Short	Directional
Fit-interactions	10-100	Short	Very selective
Amphiphilic	5-50	Short	Non-selective
<b><i>Ionic</i></b>	<b><i>50-250*</i></b>	<b><i>Long</i></b>	<b><i>Non-selective</i></b>
Covalent	350	Short	Irreversible

\* Data are for organic media, dependent on solvent and ion solution

*Table 2.1: Non covalent Interactions and some of their properties.<sup>5</sup>*

## 2.2 Literature review on Tectons:

Tectons reported in the literature have been classified into four categories where ISA strategy has been applied

1. **Geometric multivalent organic counter ions** (includes charged oligopeptides, charged inorganic clusters, polyoxometallates) where well-defined shape adds to the stability apart from multiple charged sites
2. **Surfactant-lipid systems** where the coulombic binding facilitated by hydrophobic effect and demixing phenomenon in hydrophilic and hydrophobic domains.
3. **Chromonics** which constitutes discotic systems and charged dyes where Coulombic forces was synergized by shape,  $\pi$ - $\pi$  interactions, anisotropic polarizability, and other electronic interactions
4. **Polyelectrolytes** of both organic and biological origin with repetitive functional arrangements within chains thereby promoting cooperativity.

### 2.2.1: Geometric multivalent organic counter ions:

A combination of ionic self-assembly (ISA) and classical metal coordination leads to the production of thermotropic liquid-crystalline materials. These mesogenic ISA materials, based on simple and accessible starting materials, exhibit typical phase morphologies such as lamellar and a variety of columnar phases. The phase behavior can easily be tuned by variation of the alkyl-tail volume fraction of the complexing surfactant species. There are a lot of reports of inorganic structures such as clusters and inorganic polymers which are known for their good solubility in water and polar organic solvents. The counter ion exchange with surfactant tails enhances solubility in organic solvents. These clusters are known for their supramolecular assembly behavior due to their ambipolar characters<sup>8</sup>.

Some of the widely explored clusters are germanium sulfides. Germanium sulfides on complexing with ammonium surfactants form hexagonal morphology in presence of metal cations ( $\text{Co}^{2+}$ ,  $\text{Ni}^{2+}$ ,  $\text{Cu}^+$ , and  $\text{Zn}^{2+}$ )<sup>9</sup> (**Figure1**)

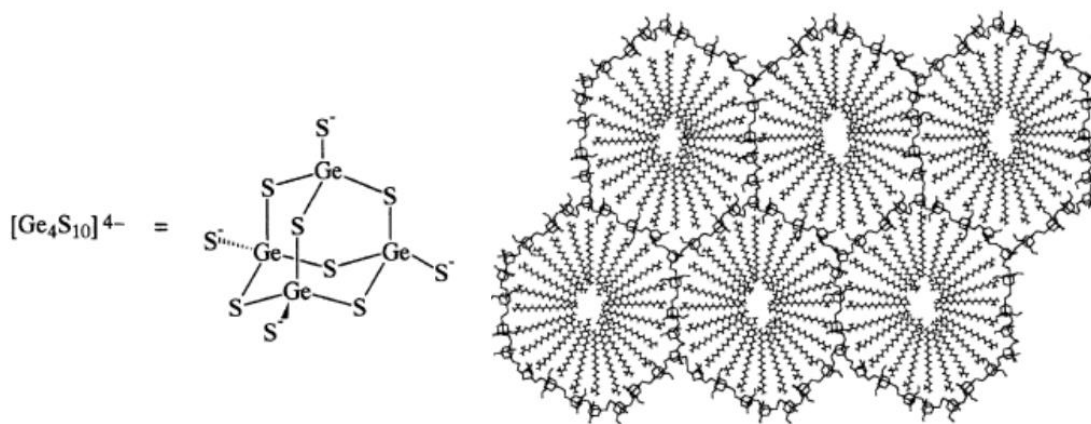


**Figure 1: Structure of germanium sulfide cluster**

#### 2.2.1.2: Polyoxometallates :

Transition-metal polyoxometallates are typical inorganic metal-oxide clusters that show diversity in both topologies and chemical and physical behavior. These inorganic clusters have been of much use in catalysis, medicine, electrodes, and materials science. A recent trend in

polyoxometallate chemistry has been the fabrication of functional nanostructures by using polyoxometallates as the inorganic building blocks, specifically using ionic self-assembly<sup>10</sup>. Polyoxometallates are one of the widely known coordination clusters involving Mo, W, and V atoms in their highest oxidation states. Their structural versatility paves way for involving them in fabricating novel materials as they have large scope in functionalization which leads to organic compatibility. Polyoxometallates have been used in the ionic self-assembly process where the liquid crystallinity is completely provided by the surfactant part, the inorganic component effectively plays the role of a solvent which follows the directions of the surfactant phase (**Figure 2**). Antoinetti et al. have explored the mesomorphic potential of many other clusters such as germanates, molybdates, Nickel-based crowns, some of them have been found to show amphotropic behavior.

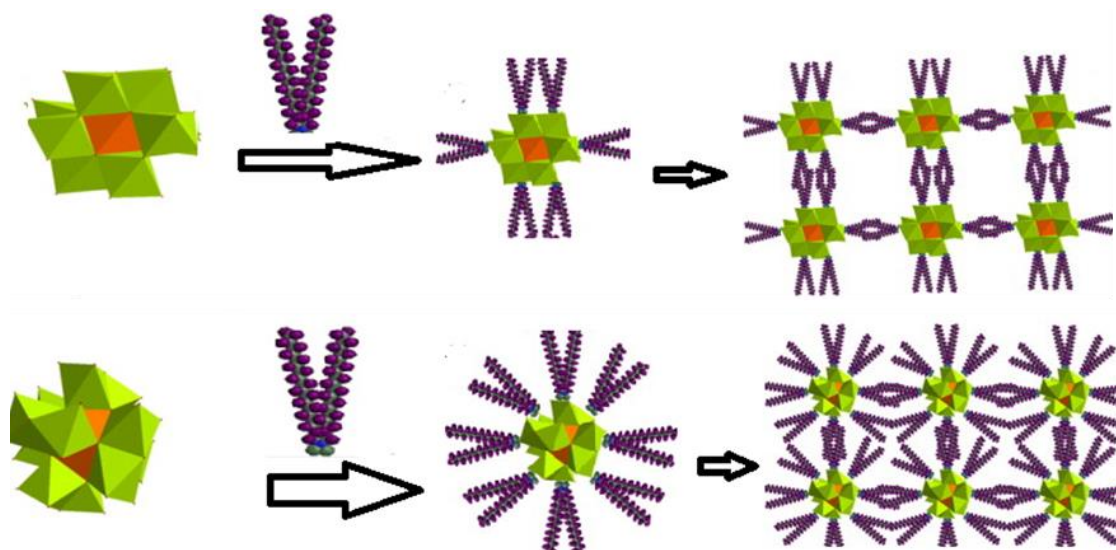


**Figure 2: Schematic of Polyoxometallates -Surfactant complex.<sup>10</sup>**

### 2.2.2 Biological tectons :

Biological systems, one of the inspirations of supramolecular chemists, have shown great scope in formation of various nanostructures. ISA strategy also showed excellent promise in the case of complexes involving biological tectons. The resultant complexes were used for various applications such as biosensing.<sup>11</sup>

ISA has been used in fabricating various nanostructures using biological tectons (**Figure 3**). This strategy was recently used for the preparation of modified electrodes (biomolecular modification on electrode surface) for various sensing applications<sup>12</sup>.

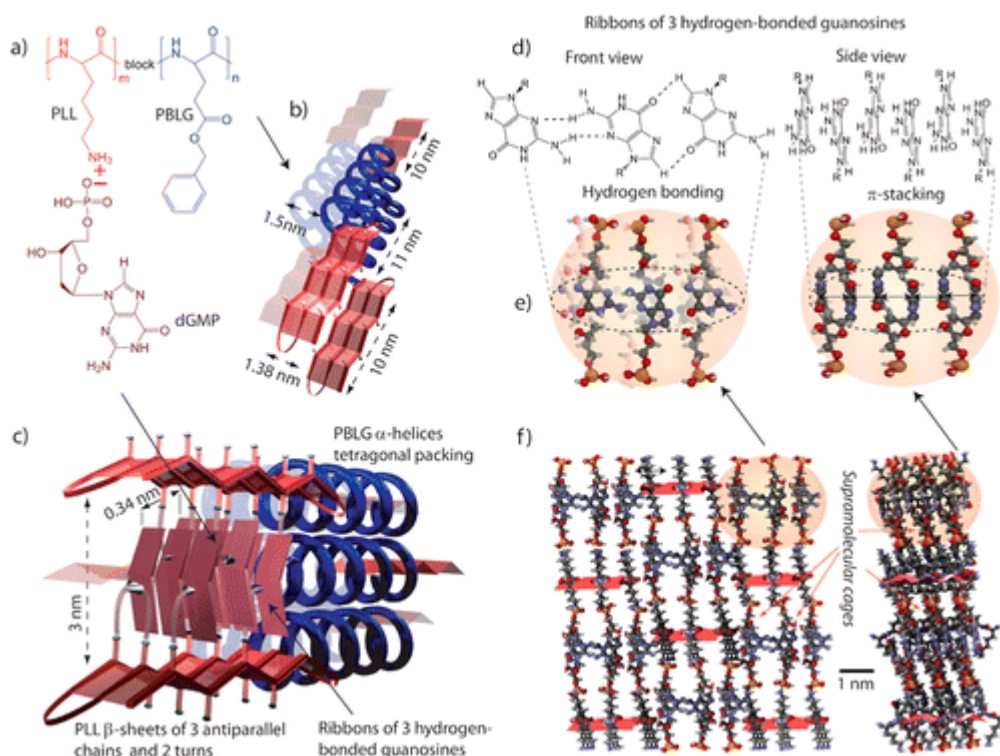


**Figure 3: Example of a biological tecton-surfactant complex involving nucleotides<sup>11</sup>**

### 2.2.3: Polyelectrolytes:

Polyelectrolyte surfactant interactions are no stranger to colloidal research<sup>13</sup>. This complexation is often driven by the release of counterions. The combination of both polyelectrolyte and surfactant is rich in their mesoscopic organization as such, on mixing they pave way for the formation of diverse structures (**Figure 4**). The morphology of complex is a function of structural parameters of both polyelectrolyte (persistent length, charge density along the chain, charge proximity to backbone, molecular weight) and surfactant (the type of head groups, type of aggregates). One of the hallmarks of these complexes is their sensitivity towards  $p^H$ , ionic strength, temperature,

pressure. These types of complexes show the tendency to form coacervates (coexistence of two liquid phases). Some of the reports of polyelectrolyte-surfactant complexes through ISA are documented in literature<sup>11,13</sup>

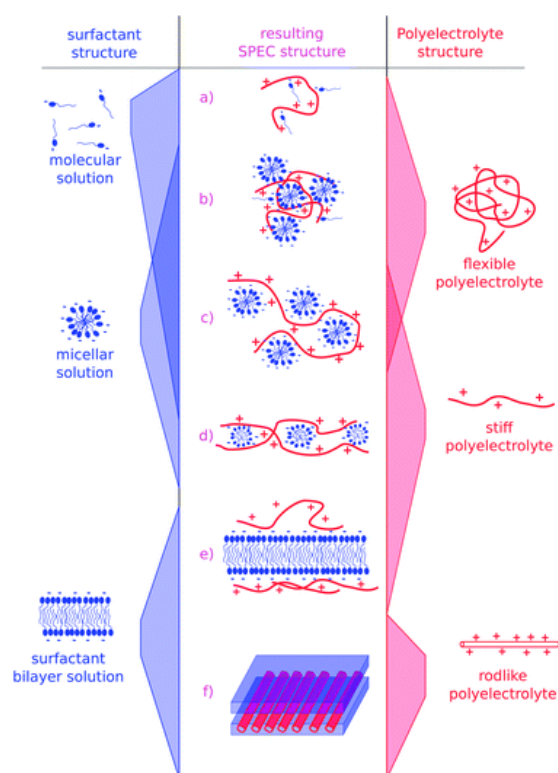


**Figure4: Types of Polyelectrolyte-Surfactant complexes<sup>14</sup>**

#### **2.2.4: Dye- surfactant complexes:**

Dye molecules are widely known for their color. They can be considered as building blocks of self-assembly. Dyes are colored because they absorb electromagnetic radiation of specific wavelength regions within the visible light spectrum more than others<sup>15</sup>. This wavelength-specific absorption originates from the presence of chromophore in molecular structures. A chromophore consists of a conjugated system, which is a group of connected  $\pi$ -orbitals. Such a conjugated system contains delocalized electrons, caused by the presence of alternating single and multiple bonds. One of the notable character of dyes is metachromasia. Metachromasia is a phenomenon

where a dye shows a distinct shift in the typical wavelength corresponding to the maximum absorbance peak(s), as a function of concentration, molecular organization and/or physical characteristics of its environment, without disturbing the chemical structure.

Polyelectrolyte-dye-complexes form spontaneously when oppositely charged polyelectrolytes and dyes come into contact. The driving force for complexation is considered to be a priori electrostatic. In case the bound dye ions are in close enough proximity, dictated by the charge distance of the polyelectrolyte, individually bound dye ions can further interact via  $\pi$ - $\pi$  interactions. There is one more possibility of dye interacting with its hydrophobic domains in the polyelectrolyte backbone. When the interaction between dye ions occurs the phenomenon of metachromasy is observed in which a distinct change is in the dye's visible absorption spectrum, generally with the appearance of a new 'metachromatic' peak. When the dye ions are too far apart to interact, the visible absorption spectrum shows no change but generally, the dye's molar extinction coefficient is lowered with respect to 'free' dye molecules. Most of the dye contains a polar part which is ionic in nature and a rigid nonpolar part. The incompatibility between the two regions enables them to assemble in different structures depending on the environment. The complexes involving dye surfactants can have complex morphologies depending on the structure of dye and surfactant chains. These complexes on comparison to the polyelectrolyte surfactant system can have more rigidity (due to the additional pi-stacking interactions among the dye motifs).

Azodyes have been one of the widely reported systems to form ISA complexes with surfactants. Antoinetti et al. have prepared some of the azo dye-surfactant complexes and found their diversity in their morphology (**Figure 5**). Further, some of them showed liquid crystalline behavior depending on their structure<sup>16</sup>.

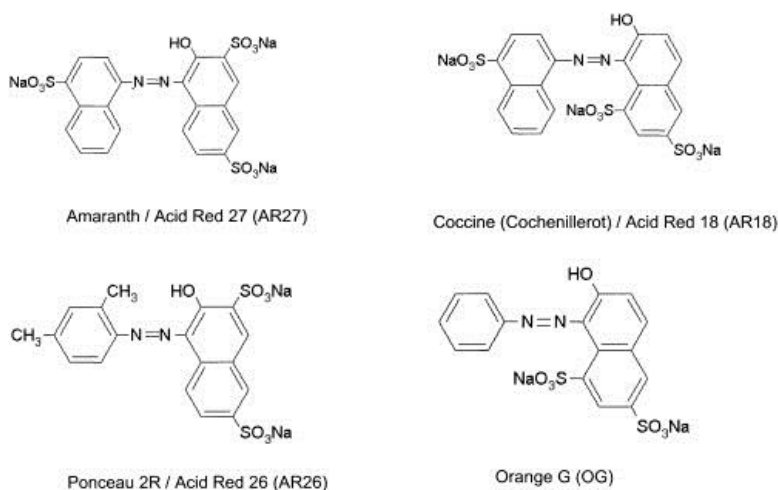


**Figure 5: Examples of Azo dyes used as tectons <sup>16</sup>.**

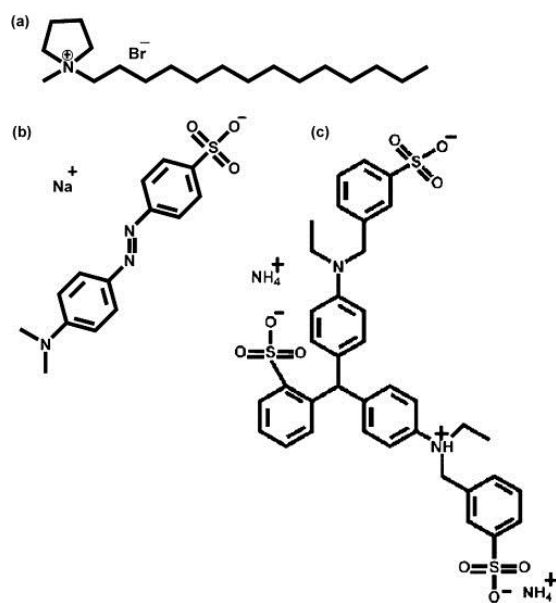


**Figure 6: Microfibers formed by ISA involving three components <sup>17</sup>**

Faul et al. have demonstrated the formation of microfibers through a simple ISA strategy, by complexation of *N*-tetradecyl-*N*-methylpyrrolidinium bromide (C<sub>14</sub>MPB) and Methyl orange (MO) with the aid of patent blue VF sodium salt (PB) molecules (**Figure 6**). The microfibers formation was found to be driven by the electrostatic,  $\pi$ - $\pi$  stacking, and hydrophobic interactions. The microfibers were fluorescent in nature<sup>17</sup>. The modified ISA strategy was employed in this case for the first time by adding the third component to induce the formation of supramolecular structures. Zakrevsky has reported optically anisotropic materials synthesized through ISA

strategy. The complex was prepared from ethyl orange dye and dialkyl dimethyl ammonium surfactants (**Figure 7**). The complexes were found to show both columnar and nematic phases as a function of temperature <sup>18</sup>.

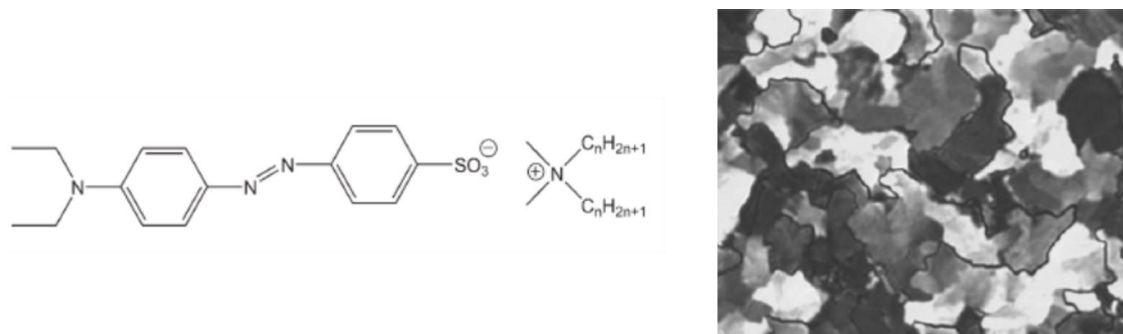


**Figure 7: Structure of ethyl orange-double tail surfactant complex<sup>18</sup>**

Faul et al. reported preparation of supramolecular polymers by adding two oppositely charged dyes through ISA strategy (**Figure 8**). The perylene diimide and copper phthalocyanines containing cationic and anionic sites respectively were used to create these supramolecular structures. It was found that apart from discotic stacking charge-transfer interactions between the two tectons facilitate the formation of helical fibers <sup>19</sup>.

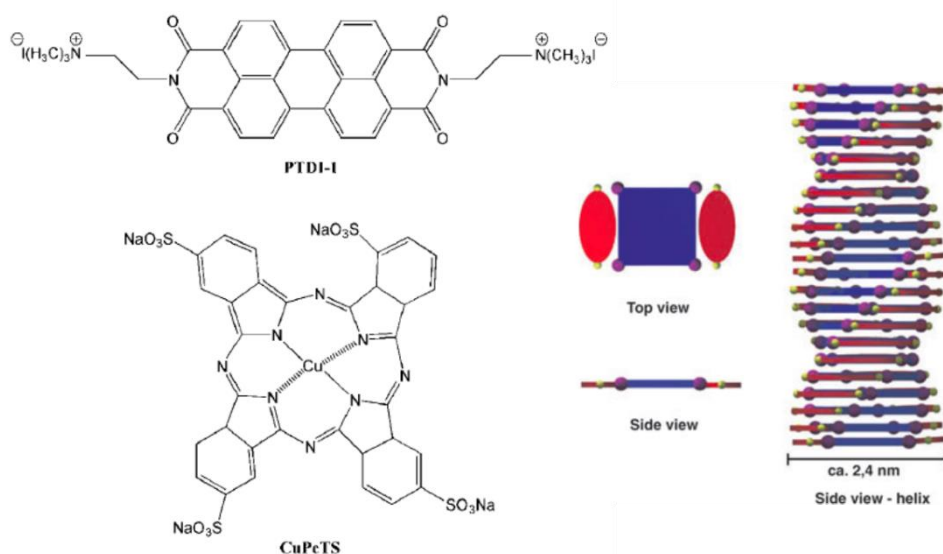


**Figure 8: Supramolecular polymers by oppositely charged dyes<sup>19</sup>**

There is a recent account of dye - surfactant complexes where the complex was formed between ferrocene based surfactant with alizarin red dye. The complexes isolated was found to be sensitive to cyclodextrin inclusion, pH, and redox species. Further, there are various other dye-surfactant complexes and their applications<sup>20</sup>.

### 2.2.5: Discotics –surfactant ISA complexes:

Discotic liquid crystals are one of the prominent types of liquid crystals where the incompatibility between the rigid core and the flexible tails induces columns like arrangement<sup>21</sup>. Disc like mesomorphic systems have been synthesized using non-covalent routes. ISA strategy has been first adopted in discotic tectons by Mullen et al. in hexabenzocoronene systems complexed with cationic polymeric systems (**Figure 9**). The resultant complex was found to be assembled in columns as confirmed through TEM<sup>22,23</sup>. This noncovalent route to mesomorphic systems has inspired many to adopt ISA strategy in creating novel architectures.

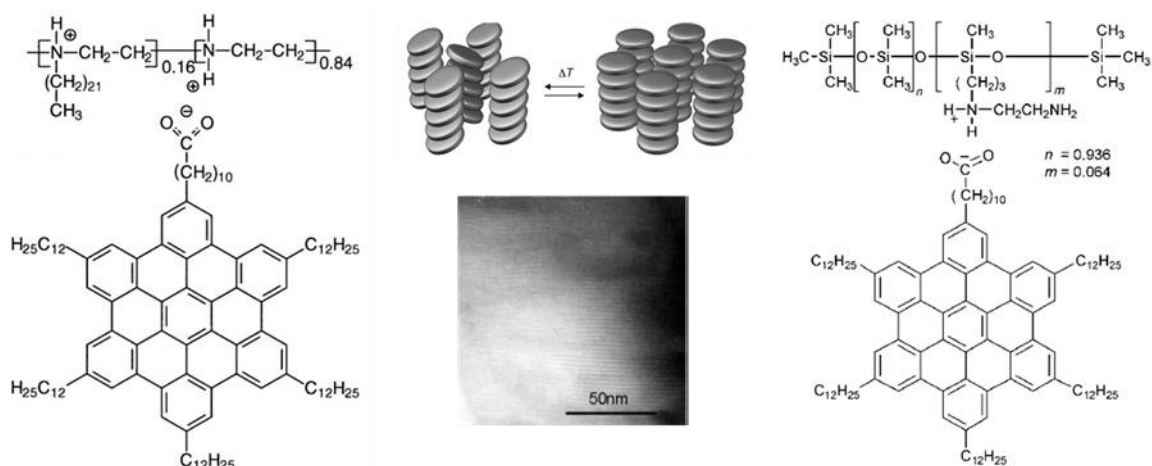


**Figure 9: Structure of ISA complex involving HBC-polyethyleneimine and polysiloxane<sup>22</sup>**

Zakrevskyy et al. have prepared ISA complexes with perylene diimide skeleton and phosphate head groups (**Figure 10**). The resultant complexes were mesomorphic. In addition to that, the shear aligned films of these complexes showed immense potential as polarizers and optical filters<sup>24</sup>.

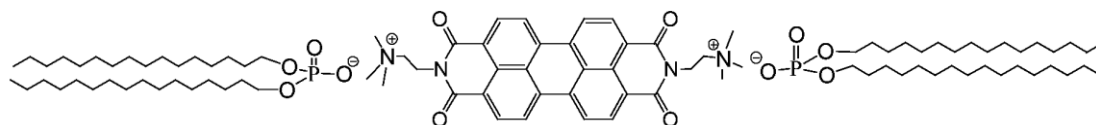


**Figure 10: Structure of ISA complex involving perylene tectons with phosphate head groups<sup>24</sup>**

Zakrevskyy et al. have reported the amphotropic behavior of perylene tecton with sulfosuccinate surfactants (**Figure 11**). The complex was found to show columnar phase<sup>25</sup>. Kadam et al. have used ISA strategy in the formation of complexes involving tricycloquinazoline and double-tailed surfactant (**Figure 12**). The complex was found to be lamellar in nature<sup>26</sup>. Faul et al. have shown the synergistic assembly involving hydrogen bonding and electrostatic interactions. The resultant complexes showed the columnar phase<sup>27</sup>. Zakrevskyy reported the smectic nature of ISA complex constituting benzene and double tail ammonium surfactants (**Figure 13**). The complex was used as a negative compensation film in-display devices<sup>28</sup>. Faul et al. have demonstrated the self-assembling behavior of Ionic self-assembled (ISA) materials obtained by the complexation of an anionic perylene bisimide dye with cationic chiral surfactants<sup>7</sup>. It was reported that the molecular chirality of the surfactants is expressed in the bisimide chromophore through the ionic linkage, clearly indicating that the surfactants act as structure-inducing moieties within the superstructures in both solution and the solid-state. In solution, the complexes form left-handed helically stacked architectures. In the solid-state, both systems are highly ordered and exhibit lamellar morphology (**Figure 14 & Figure 15**)<sup>29</sup>.

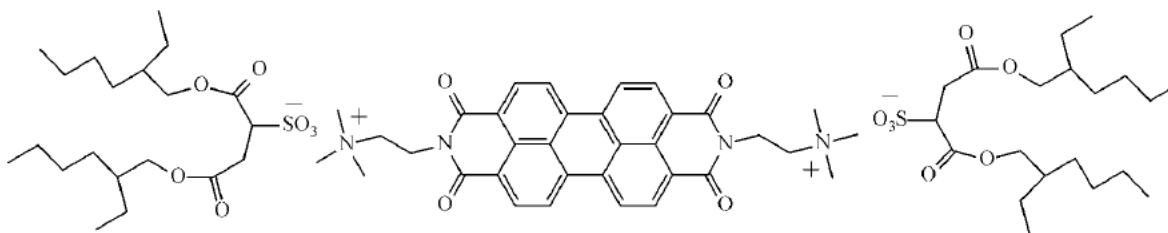


**Figure 11: Structure of ISA complex involving perylene-sulfosuccinates<sup>25</sup>**

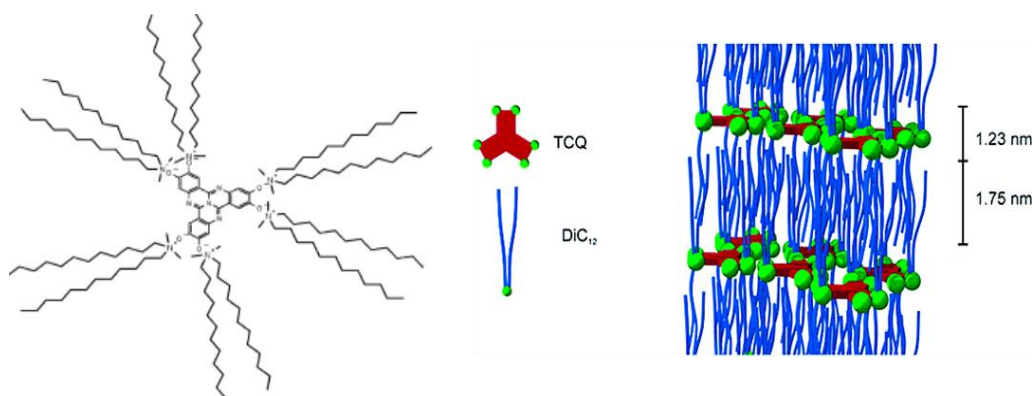


Figure 12: Structure of ISA complex involving TCQ-double tail surfactants<sup>26</sup>

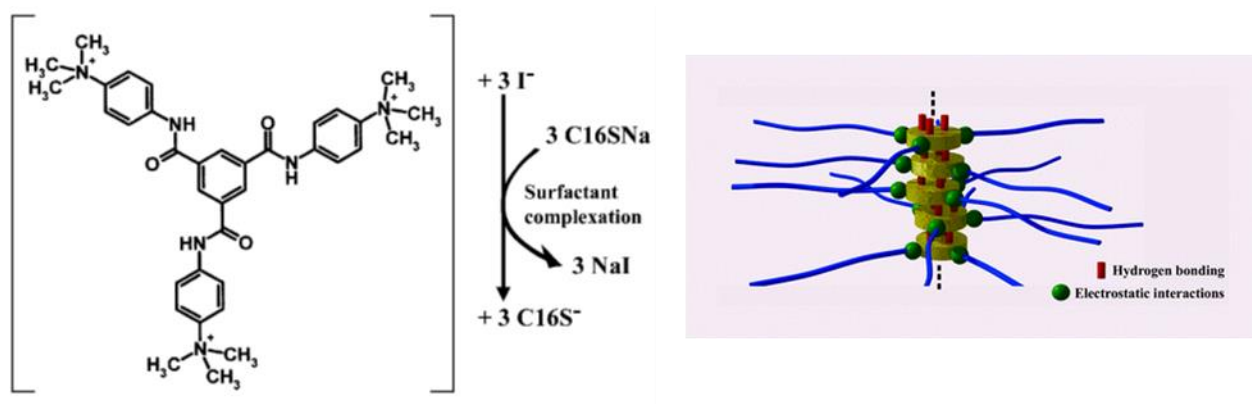


Figure 13: Structure of ISA complex involving benzenetrisamide and surfactants<sup>27</sup>

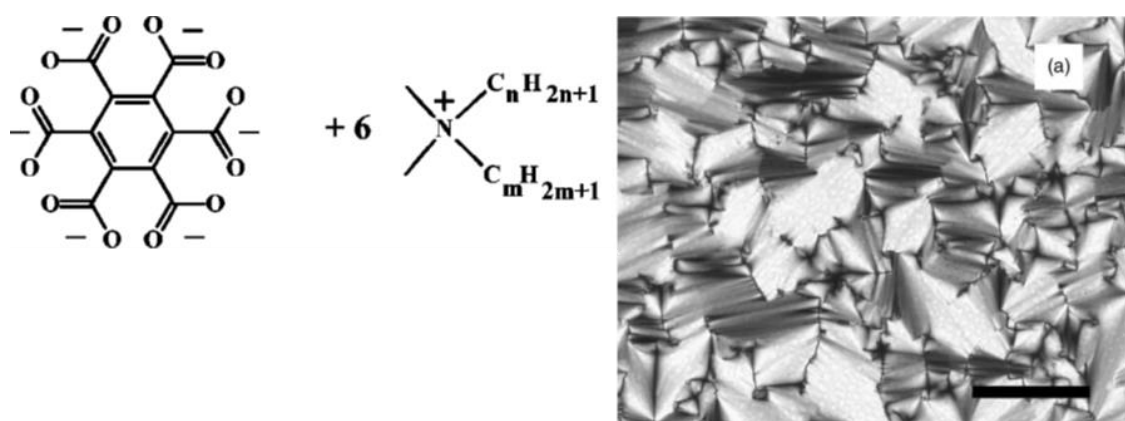
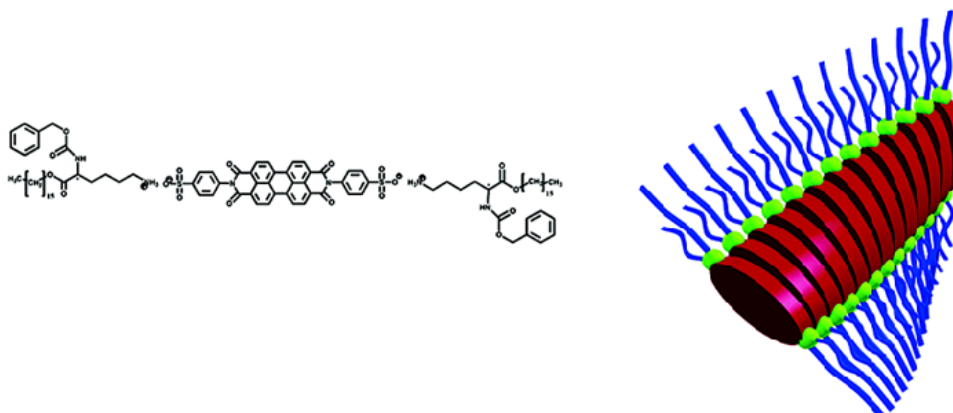


Figure 14: Structure of ISA complex involving Benzene-double tail surfactants<sup>28</sup>



**Figure 15: Structure of ISA complex involving perylene dye-chiral surfactants<sup>29</sup>**

Camerel et al. have reported the synthesis of wedge-shaped amphiphilic molecules involving porphyrins and BODIPY and ammonium head groups<sup>30</sup> (**Figure 16**). The resultant complexes were luminescent and showed hexagonal phase. Further, it was shown that the presence of amide linkage plays a vital role in the stabilization of the columnar phase. Shi et al. have prepared ISA complex constituting anionic tecton ATP and cationic perylene diimide. It was proposed that the electrostatic interaction initiates the association of tectons followed by pi-pi interactions and hydrophilic interactions suggesting cooperative binding. These cooperative binding induced the formation of optically active superstructures<sup>31</sup> (**Figure 17**).

Faul et al. have prepared a new sugar-based perylene diimide derivative and studied their assembling behavior in DMF/H<sub>2</sub>O (**Figure 18**). PTCDI-BAG molecules self-assembled into planar ribbons in 20/80 and 40/60 H<sub>2</sub>O/DMF (v/v), while left-handed helical nanowires were obtained in 60/40 and 80/20 H<sub>2</sub>O/DMF (v/v). The formation of ribbons was found to be thermodynamically controlled in the case of lower water composition systems. The higher water content system was assembled into ribbons<sup>32</sup>.

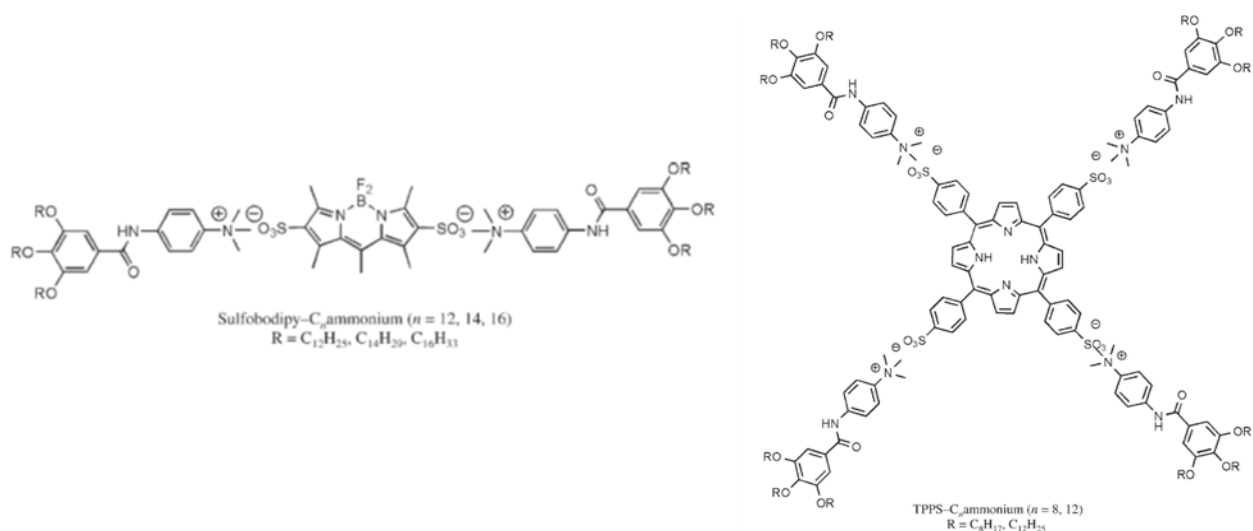


Figure 16: Structure of ISA complex involving BODIPY and Porphyrin dyes<sup>30</sup>

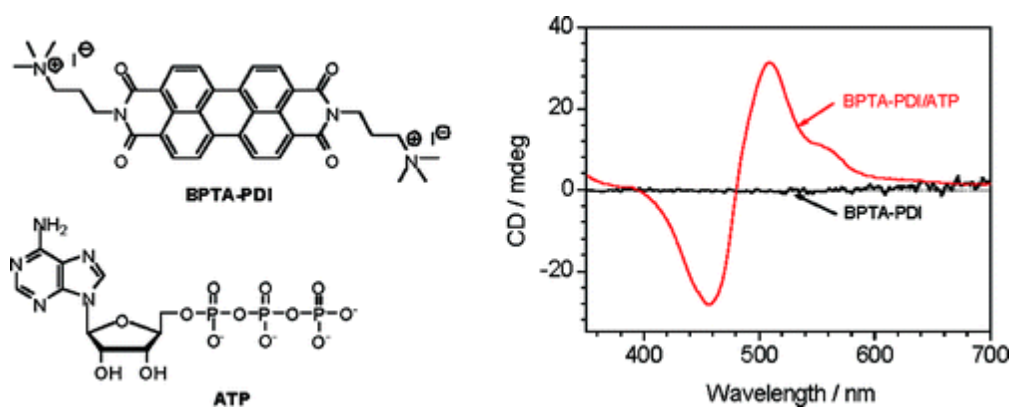
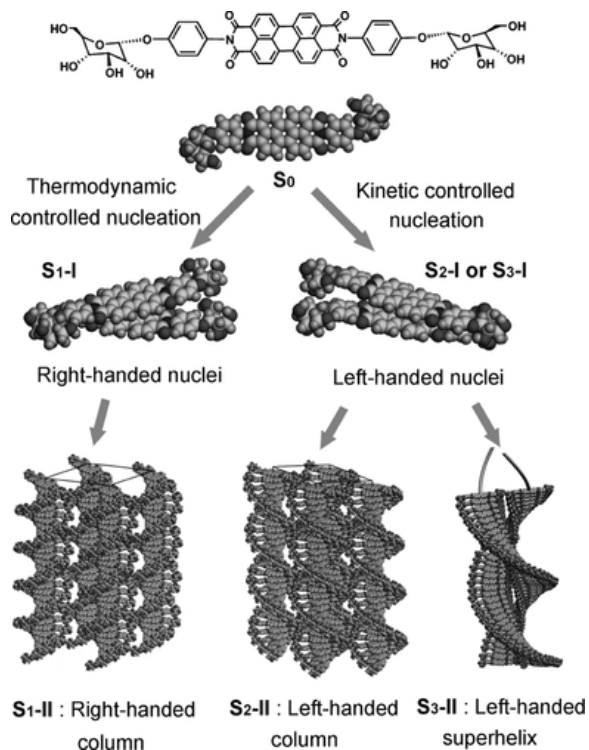
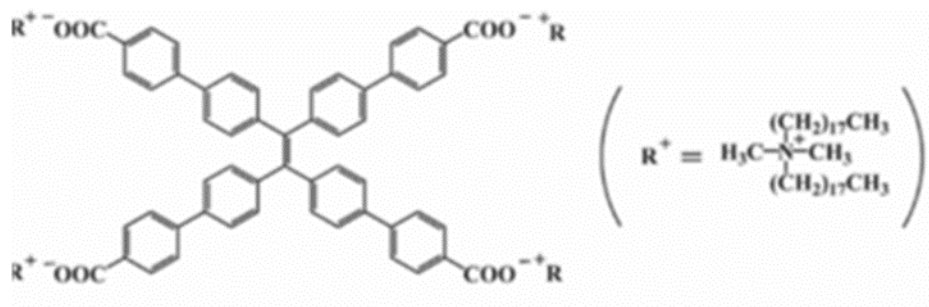


Figure 17: Structure of ISA complex involving perylene- Adenosine triphosphate<sup>31</sup>

Tetraphenylethene (TPE) is known for its aggregation-induced emission (AIE) behavior has been used as tecton. The complexation of carboxylic acid-functionalized TPE and double-tailed surfactants (DOAB) resulting in a helical supramolecular structure<sup>33</sup> (Figure 19). The resulted complex has shown enhancement in their luminescence and found to be sensitive to copper ions with a sensitivity of nanomolar concentration level.



**Figure 18: Structure of ISA complex involving perylene-sugar derivative<sup>32</sup>**



**Figure 19: Structure of TPE-DOAB complex<sup>33</sup>**

Kang et al. have reported complexation of organic cationic salt (PQPC6<sup>+</sup>) with different anions (perchlorate, anthraquinone disulfonate, benzene sulfonate) forming ordered self-assembled structures (**Figure 20**)<sup>34</sup>.

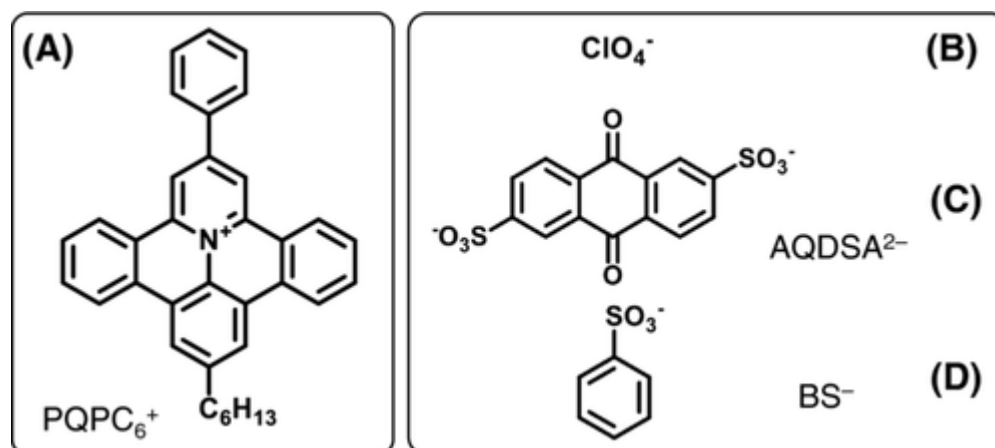


**Figure 20: Structure of PQPC6+ sulfonate complexes<sup>34</sup>**

Liu et al. have reported disc-shaped perylene polyelectrolyte with camphor sulfonic acid complex through ionic self-assembly<sup>35</sup> (**Figure 21**). The resultant complex was found to be sensitive to ethylene diamine vapors. Further, it was noticed that there are strong hydrogen bonding interactions between camphor sulfonic acid and diamine vapors that favors the sensing ability of the ISA complex. The steric effects were also found to play a role in sensing the ability of complex towards amine vapors.

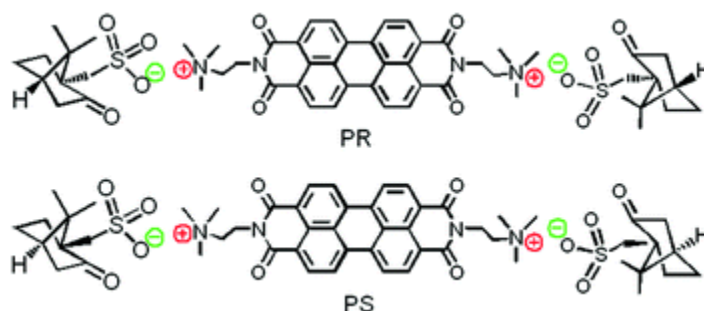


**Figure 21: Structure of Perylene-Camphor sulfonic acid complex<sup>35</sup>**

The ionic self-assembly approach was used to synthesize colloidal ionic clusters called Ionoids containing macrocyclic tetraimidazolium skeleton and anionic salts<sup>36</sup> (**Figure 22**). The complexation of rhodamine B with double-tailed surfactant (AOT) resulted in star-like materials of micrometer size<sup>37</sup> (**Figure 23**). The resultant microfibers were induced by the strong electrostatic interactions between the headgroups of both the tectons.

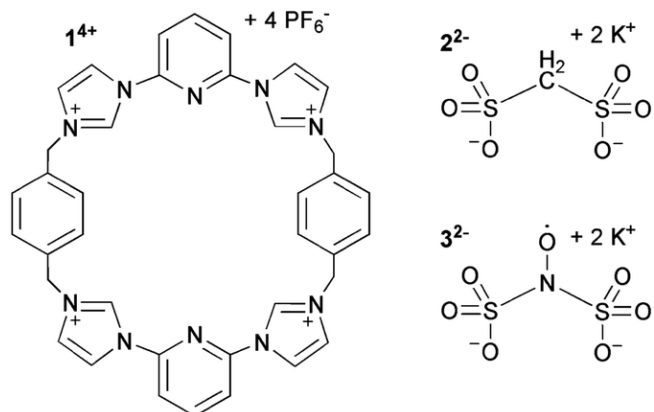


**Figure 22: Structure of tetra imidazolium-sulfonate complex<sup>36</sup>**

Giesselmann et al. have reported series of tetraguanidinium tetraphenylethene (TPE) arylsulfonates with different chain lengths (**Figure 24**) the lower homologue showed hexagonal phase whereas the higher homologue showed oblique mesophase<sup>38</sup>. The ISA approach was incorporated in both cationic and anionic porphyrins (**Figure 25**). The resultant complex was found to have excellent self-assembling behavior and has a great scope in optoelectronics. Wong et al. have formed porphyrin dimers (Figure 26) through the ISA approach involving positively charged Fe<sup>III</sup> meso-tetra (N-methyl-4-pyridyl porphyrin and negatively charged Fe<sup>III</sup> meso-tetra (4- sulfonate phenyl) porphyrin (Fe<sup>III</sup> TPPS<sub>4</sub>). The resultant complex was found to show electrocatalytic behavior for oxygen reduction reactions.<sup>39,40</sup>

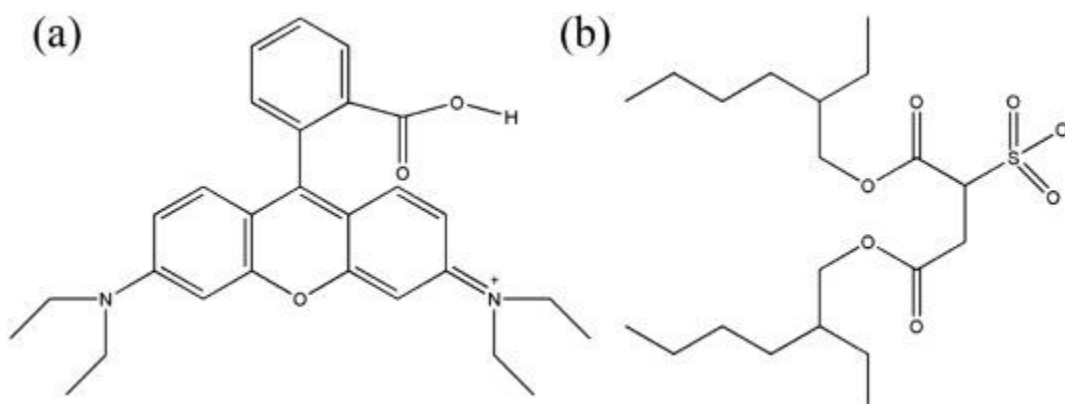


**Figure 23: Complexation between Rhodamine6-G and AOT surfactant<sup>37</sup>**

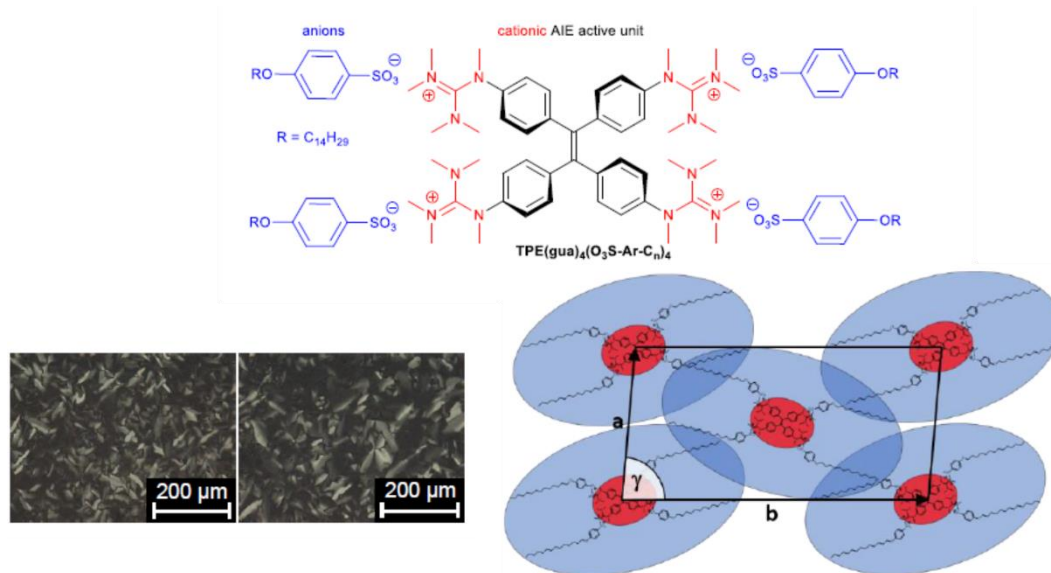


**Figure 24: Structure of TPE- guanidinium complex<sup>38</sup>**

Wang et al. have reported the ISA complexes involving dye and polyoxometallate tectons (**Figure 27**). The complexes formed lamellar vesicles and they showed excellent charge transfer behavior<sup>41</sup>

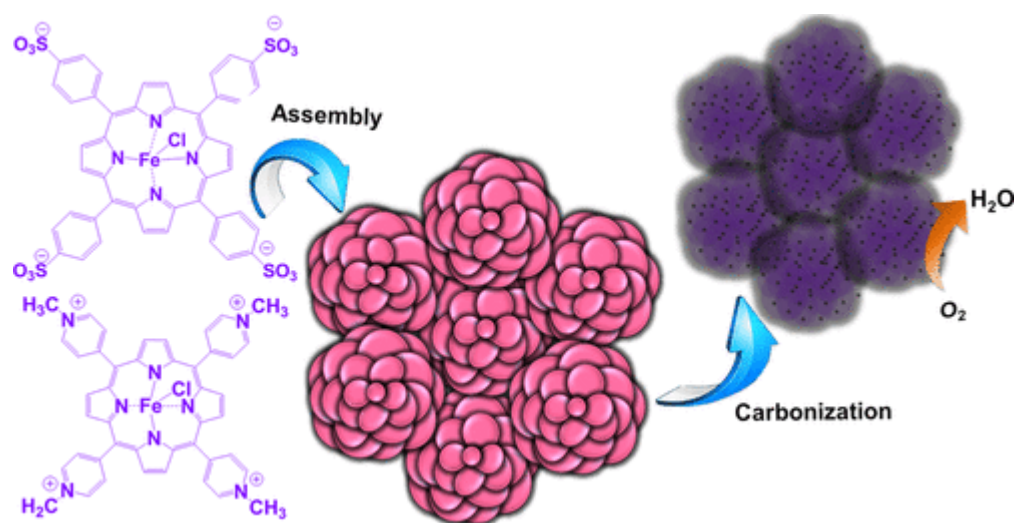


**Figure 25: Schematic of complexation of opposite charged porphyrins<sup>39</sup>**

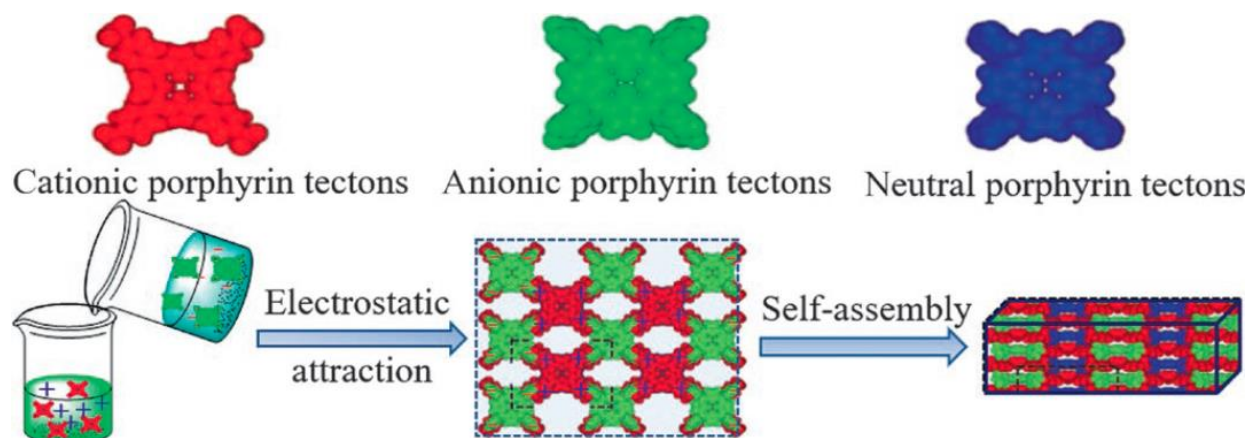


**Figure 26: ISA involving opposite charged porphyrins<sup>40</sup>**

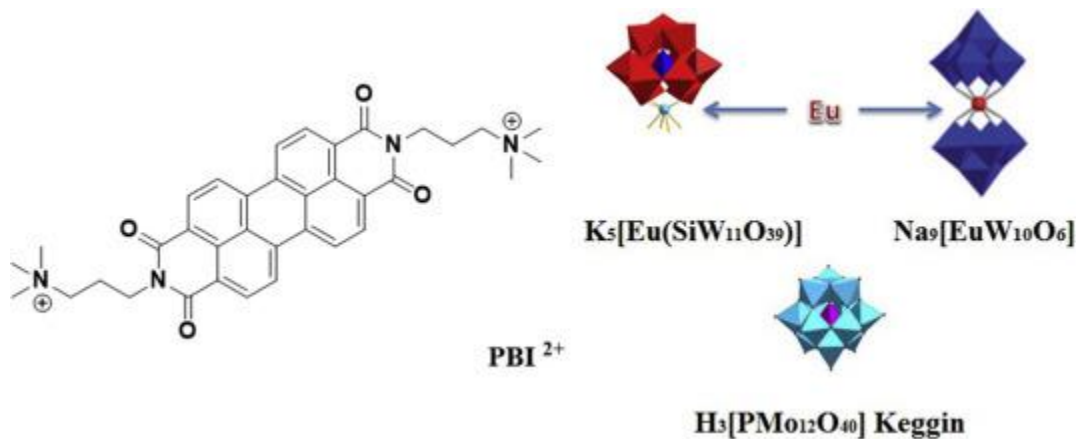


**Figure 27: structure of perylene -POM complex<sup>41</sup>**

Anthraquinone and triphenylenes are no strangers to the discotic family. Their derivatives have been found to be mesomorphic in nature. We have used both anthraquinone and triphenylene as a tecton to form ISA complexes. The complexes have been studied for their mesomorphic behavior.

## **2.3: Results and discussion:**

### **2.3.1 Anthraquinone-surfactant complexes:**

The ionic self-assembled complexes were synthesized from their corresponding acetates and surfactants in an alkaline medium. The structure of complexes are shown in **figure 29**. This method involves in situ formation of sodium salt of discotic derivatives which insitu forms an ionic complex with double tail surfactants, It was confirmed by preparing sodium salt of the hydroxy derivatives of anthraquinones (AQ) by treating with the appropriate equivalent of sodium in THF and reflux overnight, filter the precipitate wash with organic solvents and used as such. The complex formed by sodium salt and surfactant showed the same transition temperature and phase behavior. The length and number of surfactants have the influence of solubility of reactants in water. Surfactants with long alkyl tails do not readily dissolve in water. The formation of the complex was confirmed by immediate precipitation of solid, after 24 hrs the precipitated product was washed with water to ensure the removal of sodium bromide, as confirmed by analysing the washings with silver nitrate solution. Finally, the complex was dried for 24 hrs and taken for analysis. All the complexes were characterized using IR, NMR and elemental analysis. The IR spectra of AQ octaacetate and its complex with a surfactant are shown in the **figure28**. The acetate peak was completely absent in the spectrum of its complex indicating the formation of the desired complex.

The formation of the complexes was confirmed from  $^1\text{H}$  NMR spectra of all the complexes. Representative examples of the  $^1\text{H}$  NMR spectrum of complexes are shown in **Figure 30-32**. The spectrum confirms the structure of the complex. The stoichiometry of all complexes was confirmed using elemental analysis). The amount of nitrogen matches with calculated data within acceptable error limits. The amount of C and H, even after excessive water wash indicated some amount of impurities as also observed for similar tricycloquinoxaline complex by Faul *et al.* <sup>26</sup>.

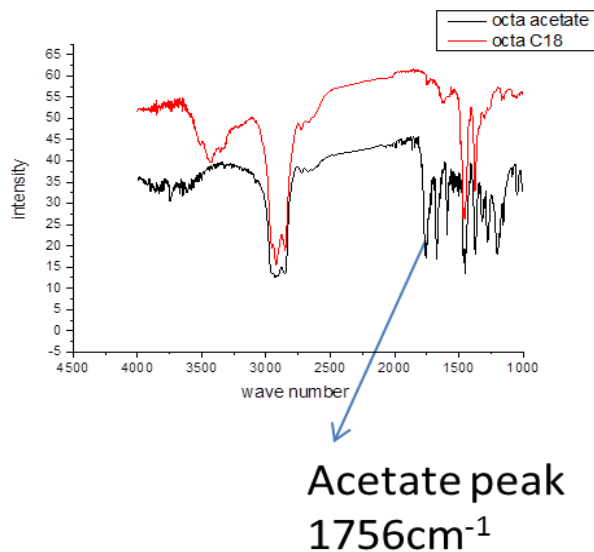


Figure 28: IR spectra of of AQ—C14 complex and Aq hexaacetate

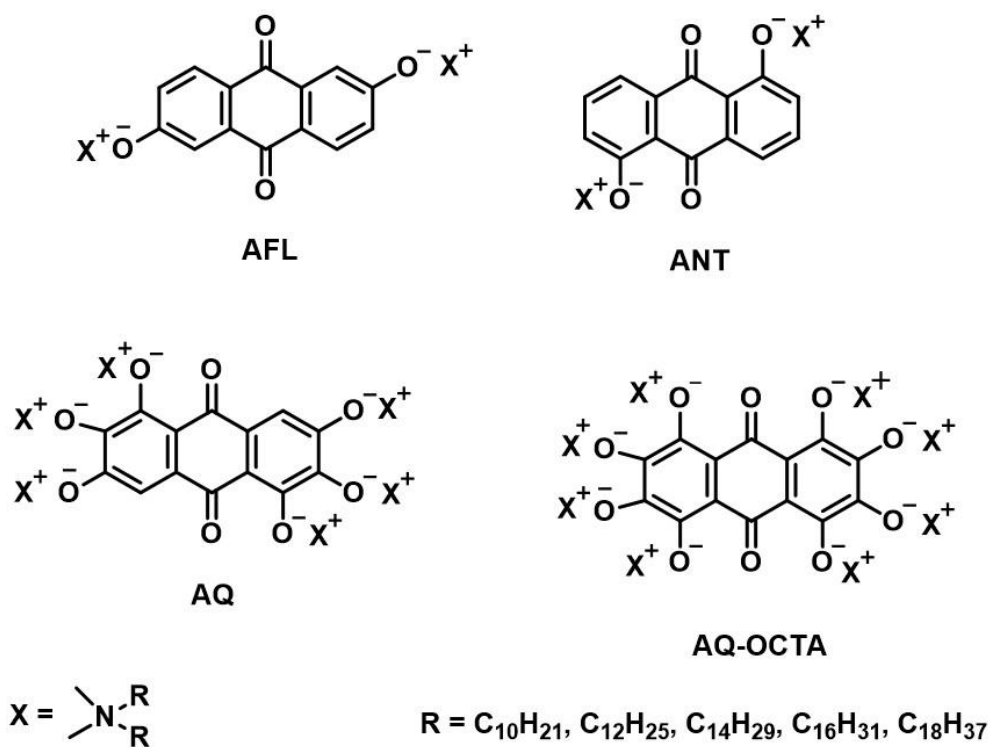


Figure 29: structure of AQ-ISA complex

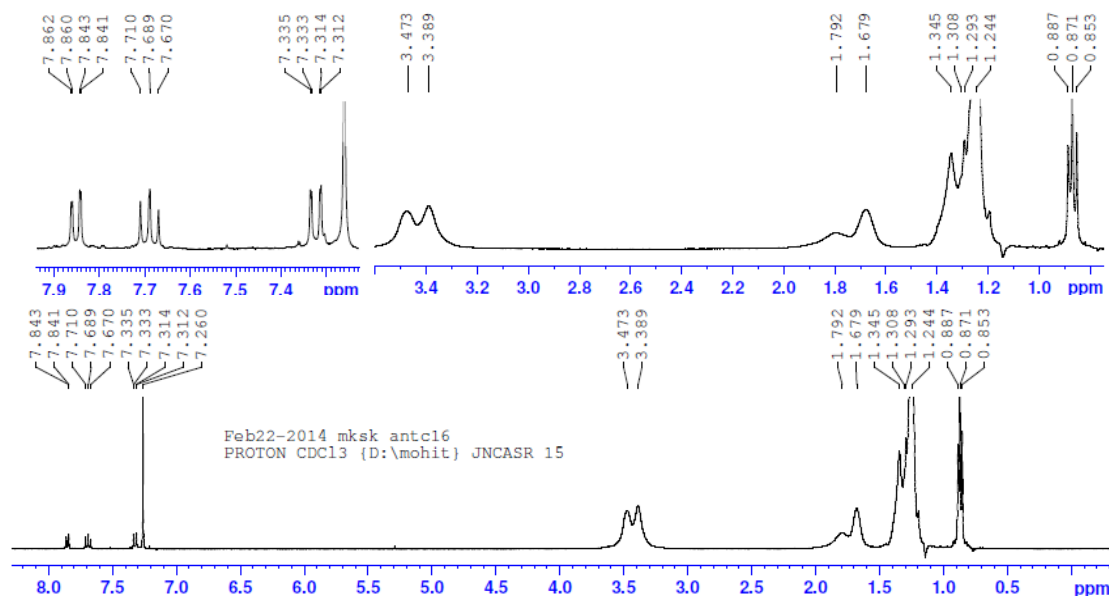


Figure30:  $^1\text{H}$  NMR spectrum of complex ANT C16 (full spectrum and expanded version on top).

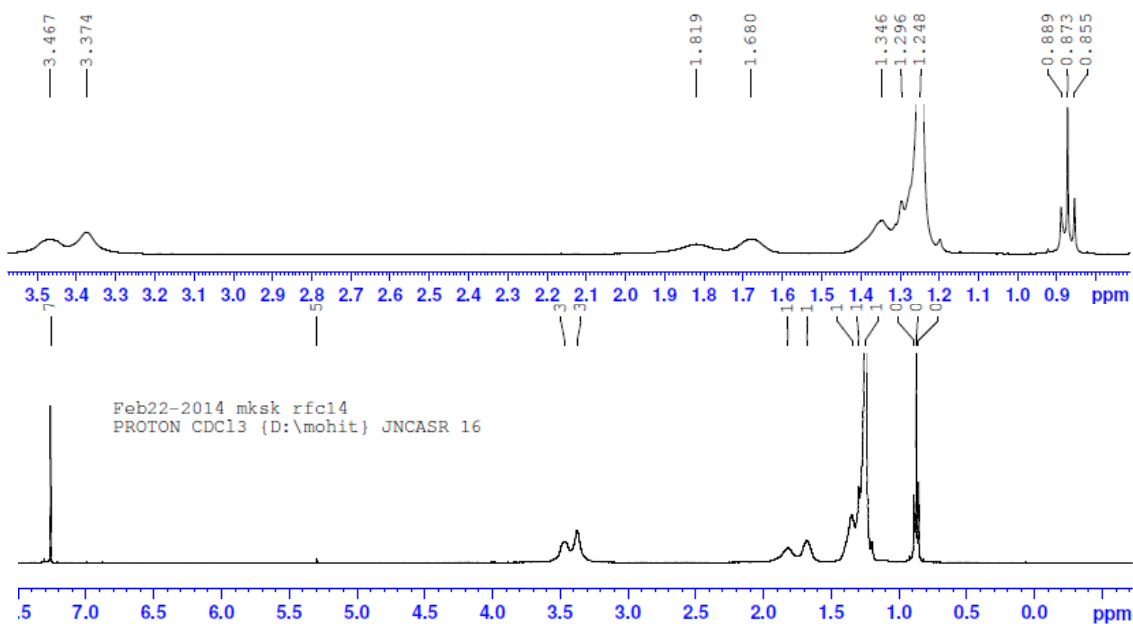
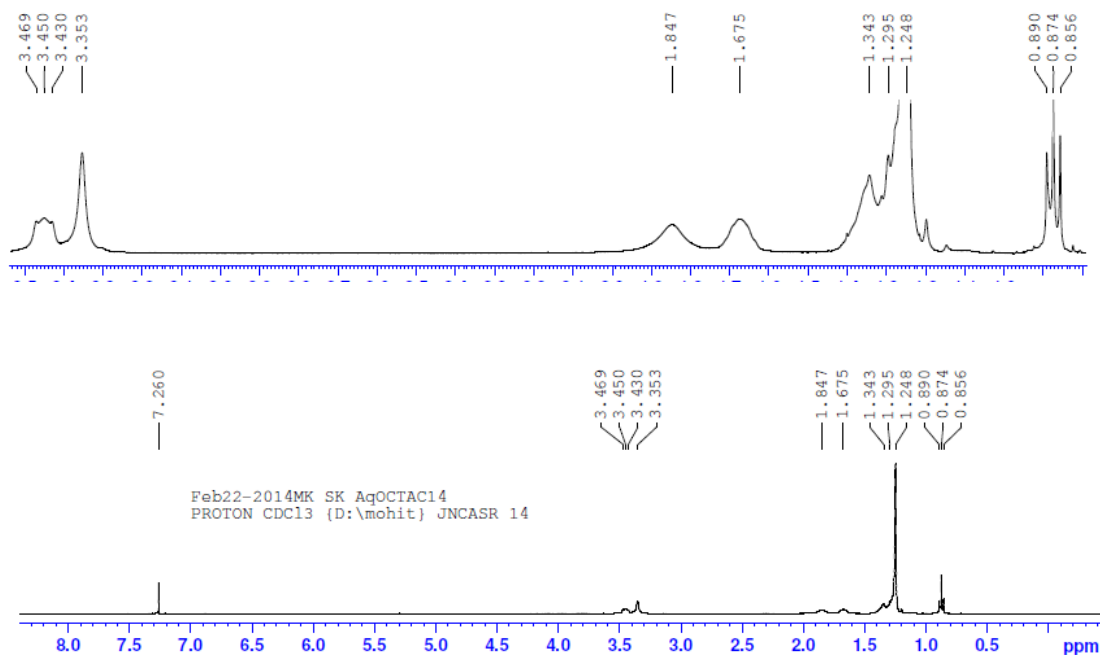


Figure31:  $^1\text{H}$  NMR spectrum of complex AQ C14 (full spectrum and expanded version on top).



**Figure 32:  $^1\text{H}$  NMR spectrum of complex AQ OCTA C14 (full spectrum and expanded version on top)**

### 2.3.1.1 Elemental analysis of complexes :

The composition of complexes was analysed using elemental analysis (Table 2.2). The analysis of CHN data was analyzed as follows.

$$n_s = N \quad (1)$$

$$n_c O_c = O \quad (2)$$

$$n_s C_s + n_c C_c = C \quad (3)$$

$n_s$  = no of moles of surfactants

$n_c$  = no of moles of cores

$C_s$  = no of carbons in surfactants

$C_c$  = no of carbons in core

On solving three simultaneous equation we get the ratio between no of moles of cores and no of moles of surfactants.

The equations were designed in such a way that the oxygens present in the complex are coming from the core. This will give an idea about number of tectonic sites associated with the core. The nitrogen content in the complex has been contributed by the surfactants. The amount of nitrogen

tells us about the number of surfactants. The relative ratio gives an idea about the stoichiometry or composition of complex approximately.

Mesomorphic properties of these complexes were studied using polarising optical microscopy (POM), differential scanning calorimetry (DSC), small-angle X-ray diffraction (SAXS). POM images showed streaks which are typical of lamellar structure. POM images of some complexes at different temperatures are shown in **Figure 33**. The complexes prepared using dodecyl dimethyl ammonium bromides were also exhibited mesomorphism. But they were very hygroscopic so it was difficult to handle them for their mesophase characterization. POM studies suggest that they were lamellar in nature. The LC behavior was further confirmed by differential scanning calorimetry. **Figure 34** represents the DSC thermograms of **ANT18**, **AFL14**, **AQ18** and **AQ Octa14**. Based on DSC and POM results, the mesomorphic behaviour of these complexes is summarized in Table 2.3

( $N_N$ - number of nitrogens in the compound;  $n_N$ =number of moles of nitrogen;  $n_o$ =number of moles of oxygen;  $n_N*N_n$ =total moles of nitrogen)

SAMPLE	C	H	N	O	$N_N$	$n_N$	$n_o$	$n_N*N_n$	N/O	$n_o*(N/O)$	$N_o$
AQOCT AC18	68.91	12.21	2.12	16.76	8	0.1514	1.047	1.2112	0.126	0.1324	9.14
AQOCT AC16	67.20	11.96	2.23	18.61	8	0.1592	1.163	1.2736	0.119	0.1393	9.14
AQOCT AC14	69.28	11.72	2.31	16.69	8	0.1650	1.043	1.3200	0.138	0.1443	9.14
AQOCT AC12	67.25	10.82	2.84	19.09	8	0.202	1.193	1.616	0.148	0.1773	9.10
AQC18	73.24	14.24	2.42	10.1	6	0.172	0.631	1.032	0.239	0.1511	6.82
AQC16	73.94	17.67	2.43	5.96	6	0.173	0.372	1.038	0.407	0.1514	6.85
AQC14	70.34	14.44	2.44	12.78	6	0.174	0.798	1.044	0.190	0.1516	6.88
AQC12	69.18	14.25	2.24	14.33	6	0.16	0.895	0.96	0.156	0.1396	6.87
ANT C18	67.56	10.65	2.36	19.43	2	0.168	1.214	0.336	0.121	0.1468	2.28
ANT C16	74.02	11.87	1.85	12.26	2	0.132	0.766	0.264	0.150	0.1149	2.29
ANT C14	73.42	11.74	2.14	12.7	2	0.152	0.793	0.304	0.168	0.1332	2.28
ANT C12	71.86	11.10	2.31	14.73	2	0.165	0.920	0.330	0.156	0.1435	2.29
AFL C18	68.26	10.92	2.44	18.38	2	0.174	1.148	0.348	0.132	0.1515	2.29
AFLC16	74.02	11.87	1.85	12.26	2	0.132	0.766	0.264	0.150	0.1149	2.29
AFLC14	71.29	11.13	2.1	15.48	2	0.150	0.967	0.30	0.138	0.1334	2.24
AFL C12	70.38	10.91	2.26	16.45	2	0.161	1.028	0.322	0.137	0.1408	2.28

*Table 2.2 Elemental analysis of complexes*

### 2.3.1.2 X-ray diffraction results:

The supramolecular organization of ISA complexes was studied using small-angle X-ray scattering (SAXS). The X-ray patterns of ANT and AFL complexes show sharp peaks in the small-angle region whose spacings are in the ratio of 1:1/2:1/3 and broad and sharp peak in wide-angle region. X-ray patterns were recorded for both heating and cooling cycles. (**Figure 35**) The small-angle peaks in the ratio 1:2:3 suggests lamellar packing in the LC state, which is further confirmed by POM images. The d spacings are given in **Table 2.4** The broad peak in the wide-angle region corresponds to the average separation between fluid alkyl chains. The sharp peak in wide angle was speculated to be coming from core-core separation. In support of this conclusion, it was found that the parent compound also exhibits a sharp peak at the same position. (**Figure 36**) ( $d=4.3\text{\AA}$ ).

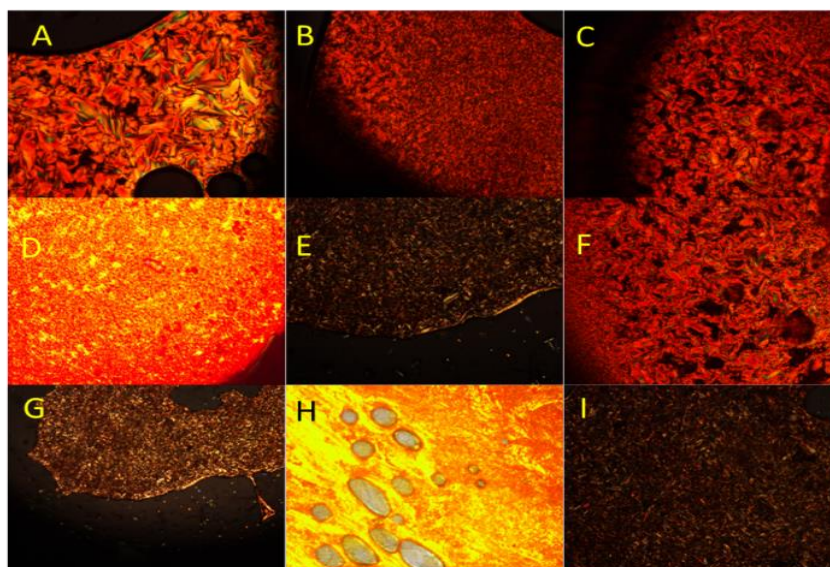


**Figure 33:** Optical textures (all images taken under 10X magnification under crossed polariser) for (a) ANT C18 at 95 °C, (b) AFL C14 at 65 °C, (c) AqC16 at 100 °C (d) Aqocta C12 at 80 °C, (e) ANT C12 at 70 °C, (f) AFL C16 at 82 °C, (g) AqC14 at 115 °C, (h) Aqocta C18 at 117 °C (i) ANT C16 at 111 °C

AQ and AQ OCTA series compounds show sharp peaks in the small-angle region with spacings in 1:1/2:1/3 ratio and a broad halo in the wide-angle region. Diffraction data were taken at every ten-degree interval. From the above results, we can confirm that these two series exhibit lamellar mesomorphism. The sharp peaks are absent in these cases, indicating no well-defined core-core separation. The spacings are given in **table 2.4**.

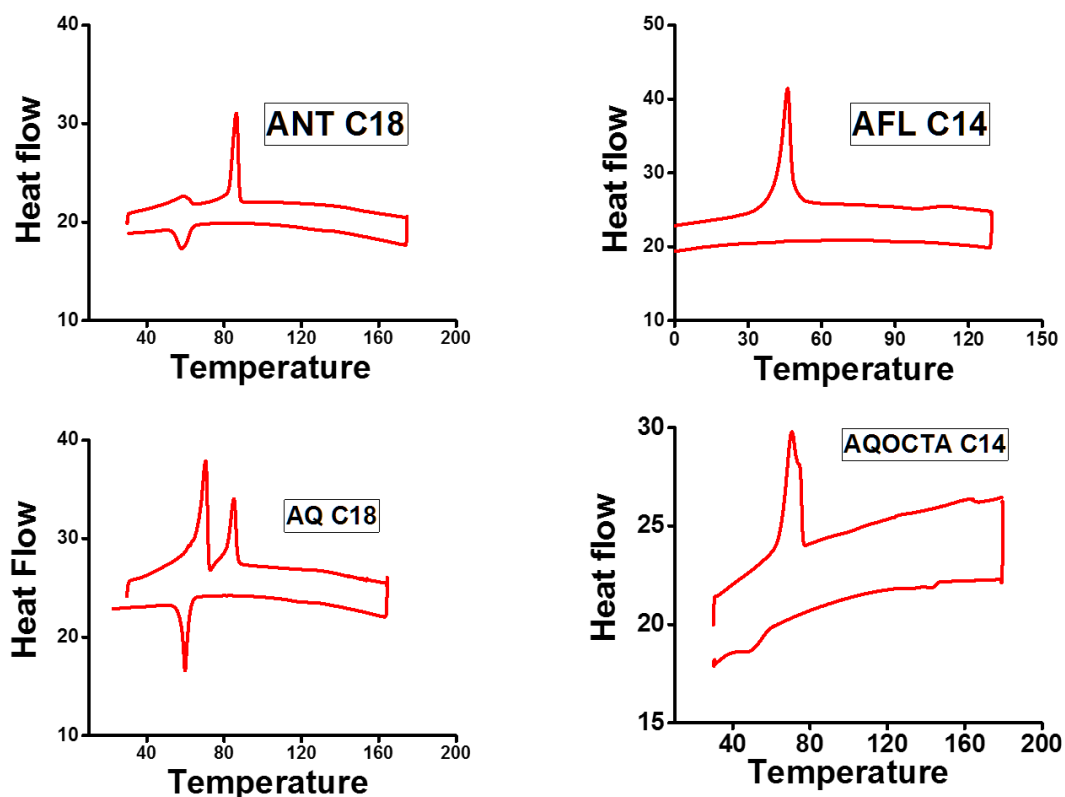


Figure 34: DSC thermogram of AQ complexes

### 2.3.1.2.1 Lyotropic mesomorphism:

The ionic self-assembled complexes were analyzed for their lyotropic behaviour in the presence of water. In order to analyze the lyotropic behaviour, the isolated complex was taken and mixed with water and taken for SAXS analysis. SAXS data show that d spacings of both hydrated complex and pure complexes are identical. This is due to the fact that as the complex is already in charge neutralized state, water is not able to swell the material. We have also studied an equimolar mixture of salt and surfactant at different water content. We took only C12 as the representative in all series of complexes for lyotropic characterization.

AQ and AQOCTA systems show diffraction patterns corresponding to the lamellar phase with one sharp peak and one or two weak peaks in the small-angle region and a broad peak in the wide-

angle region corresponding to d spacing of 4.5 Å (**Figure 37 & Figure 38**).

ANT and AFL sodium salt and DDAB were mixed with ANT alkoxide and DDAB complexes were prepared with different weight percentages, and SAXS measurements were performed. The lower composition i.e 40% water showed two sets of peaks in small angle region in SAXS where the intensity of one set of peaks varies but the second set remains the same with temperature. The POM texture shows lamellar streaks. But higher percentage water i.e. 70 % water mixture show SAXS pattern typical of  $L\alpha$  phase with no sharp peaks. Since the only difference between the two samples is the concentration of salt (NaBr) in solution, we have added salt to 70% water system to make salt concentration as that of 40% water. The SAXS pattern was found to be the same as 40% water sample i.e additional peaks appeared in SAXS as observed for 40% system. (**Figure 39 & Figure 40**)

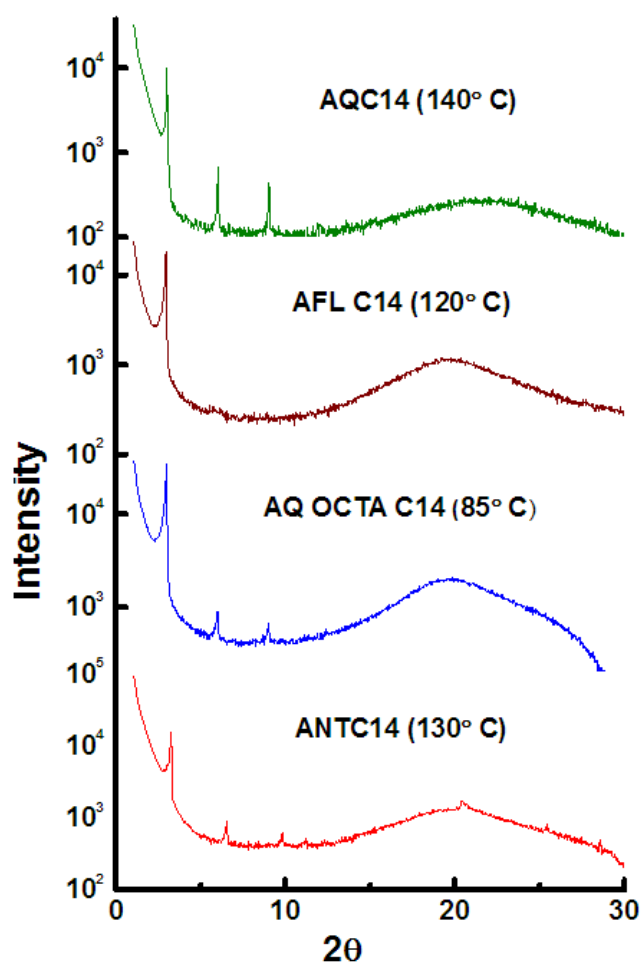


**Figure 35: Representative X ray diffractograms of complexes in the lamellar phase**

compound	Heating cycle	Cooling Cycle
ANT C14	Cr 71.02(85.15) M 146.1(2.427)	I 137.10(2.625) M 47.42 (29.75)Cr
ANT C16	Cr 45.42(88.46)Cr <sub>2</sub> 66.41(7.33)Sm152 (3.1233) I	I 143.78(1.35) Sm 58.26 (37.5)Cr
ANT C18	Cr 50.09(17.24) Cr <sub>2</sub> 82.44(83.88) Sm (2.1687 )148 I	I 135.7(0.236) Sm 58.26 (37.5)Cr
AFL C12	Cr 119.53(28.72) Sm 140.48(0.4213)I	I 128.34 (3.72)Sm 111.54(28.45)Cr
AFLC14	Cr 46.08(128.57) Sm 98.2(3.22) I	I 94.58(0.83) Sm -1.46(4.22) Cr
AFL C16	Cr 61.78(123.05)Sm 90.61(8.77)I	I 66.71(3.58) Sm 50.2(17.88)Cr
AFL C18	Cr 63.3(67.35) Sm 145.78(0.11) I	I 121.74 (1.09)Sm55.05(13.82) Cr
AQ C12	Cr 33.29(59.9) Cr <sub>2</sub> 72.84 (1.92) Sm 128 (3.01) I	I 125.92(2.88) Sm 46.2(1.00) Cr
AQ C14	Cr 43.84(128.37) Sm 70.86(4.76) I	I 60.1 (3.49)Sm 50(2.73) Cr
AQ C16	Cr <sub>1</sub> 66.02(123.58) Cr <sub>2</sub> 85.89(17.7) Sm 153.30 I	I 144.6(2.03) Sm51.37 (22.14)Cr
AQ C18	Cr70.32(37.5)Cr <sub>2</sub> 87.02(68.54) Sm 137.52(0.38) I	I 127.16(2.92) Sm 60.25(42.02) Cr
AQ OCTAC12	Cr 62.17 (79.194)Sm 156.84(3.45 ) I	I 152.58(4.56) Sm44.91(5.78) Cr
AQOCTA C14	Cr 64.55(86.21) Sm 159.45( 1.71)I	I 136.6 (1.92)Sm 49.65(10.34) Cr
AQ OCTA C16	Cr 66.51 (115.2)Cr <sub>2</sub> 86 (17.29)Sm 166.10 (2.97)I	I 145.93 (2.95) Sm 54.59 (25.85)Cr
AQOCTAC18	Cr 87.39(88.53) Sm 149.27(2.16) I	I 127.1(1.74) Sm 57.76(40.78) Cr

**Table 2.3: Thermal behaviour of AQ complexes**

Compound	d spacings
<b>AFL14</b>	29.49, 4.5 (sharp)
<b>AFL16</b>	33.42(10),16.76(20),11.19(30), 4.49
<b>AFL18</b>	36.2(10),18.39(20),4.46,3.70 (sharp)
<b>ANT C14</b>	27.13(100),13.51(200),9.01(300),7.9(400),4.43(sharp), 3.5,3.12
<b>ANT C16</b>	27.50(100),13.04(200),9.14(300),7.92(400),4.32(sharp),4.65,4.92,3.5,3.12
<b>ANT C18</b>	34.34 (100),17.08(200),11.35(300),4.30(sharp)
<b>AQ12</b>	27.56(100),13.82(200) 4.42
<b>AQ14</b>	29.4(100),14.65(200),9.74(300),4.31
<b>AQ16</b>	30.58(100),15.29(200),10.16(300),4.30
<b>AQ18</b>	34.69(100),16.99(200),11.33(300), 4.49
<b>AQ Octa12</b>	25.8(100),12.89(200) 4.49
<b>AQ Octa14</b>	29.24(100),14.56(200), 9.62(300),4.42
<b>AQ Octa16</b>	30.55(100),15.28(200), 10.16(300),4.31
<b>AQ Octa18</b>	37.38(100),18.69(200), 12.40(300), 4.49

*Table 2.4: d-spacings of complexes*

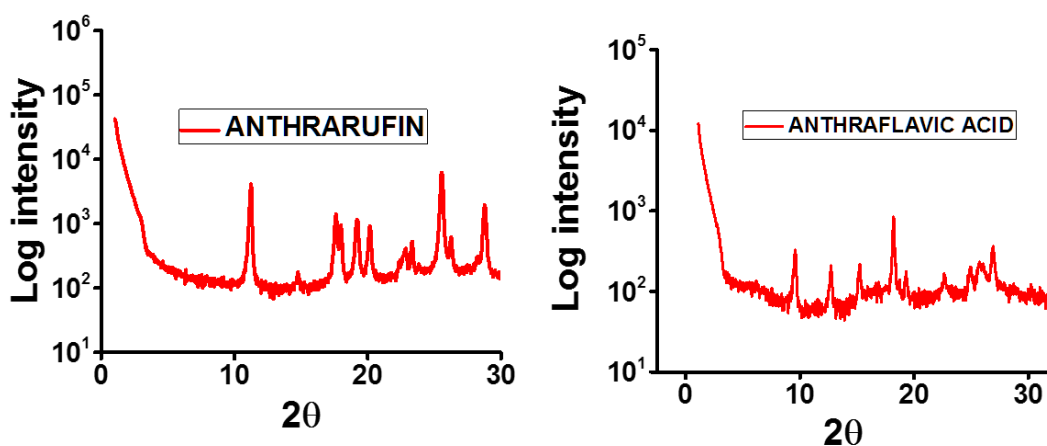


**Figure 36 : X ray diffractograms of anthrarufin and anthraflavic acid at room temperature**

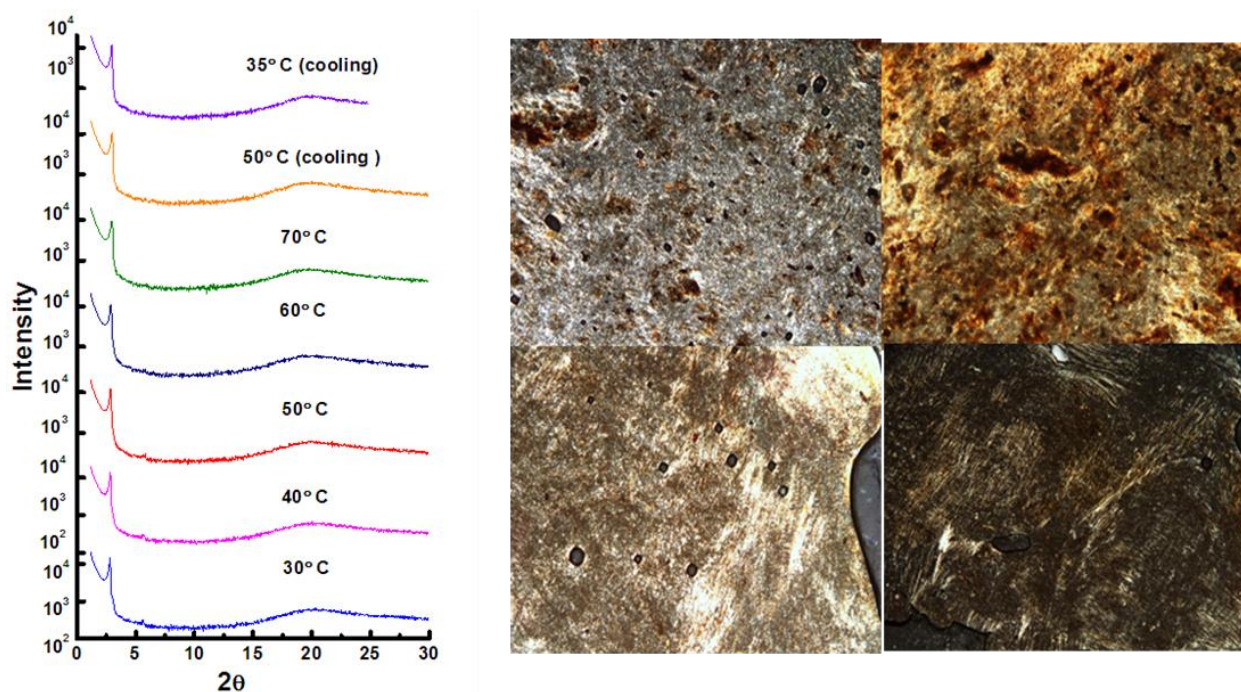


Figure 37: POM & diffraction patterns of AQOCTA-C12 70% water system

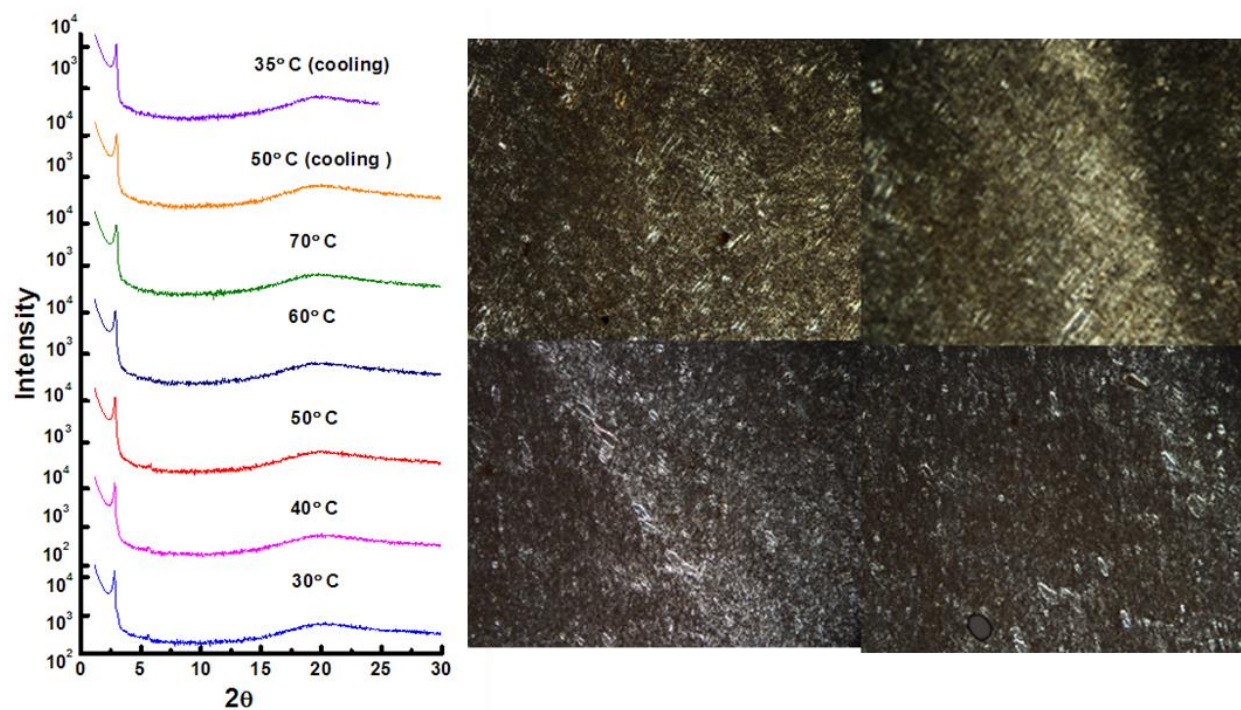
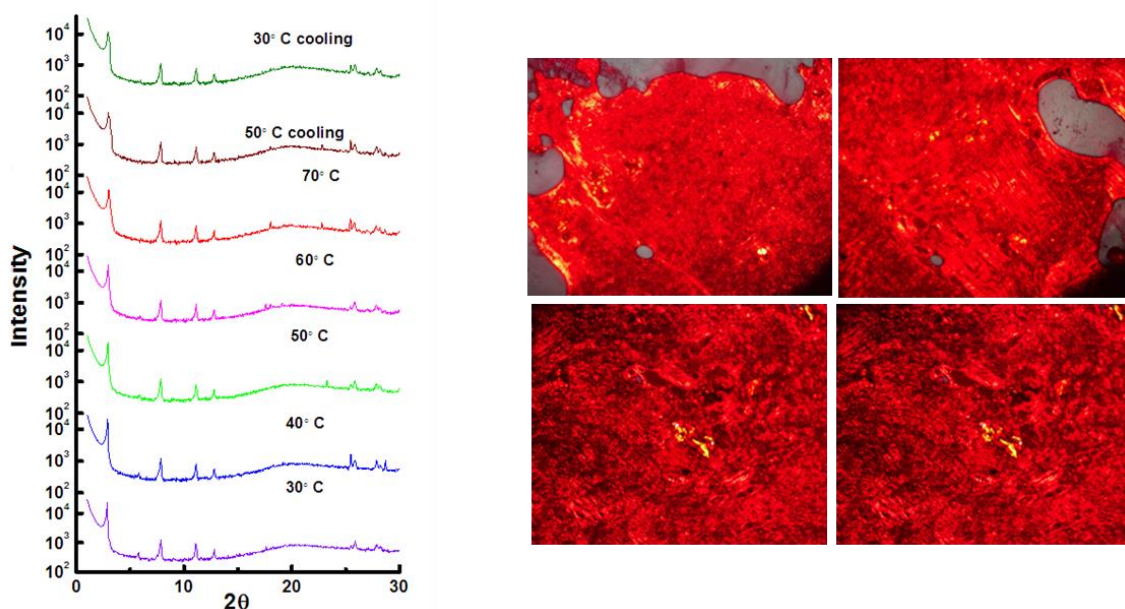


Figure 38: POM & diffraction patterns of AQ-C12 70% water system.

It was found that sodium salt of ANT and AFL can be salted out from NaBr solutions of concentrations around 2.5M which is the concentration of released salt in the 40% water system. The diffraction pattern of salted out crystallites matches very well with additional peaks seen in the 40% water system (**Figure 41**).

Not all the AQ tectons are sandwiched within the lamellar phase; some of them are found to be in the supernatant. However, when NaBr concentration becomes high they are salted out. DDAB forms bilayers with some of the AQ ions sandwiched between them. In the case of 40% water ANT and AFL systems, salt crystallites are dispersed within the above lamellar phase giving rise to the additional sharp peaks in the diffraction pattern. In case of AQ and AQ OCTA system, since they have 6 and 8 charged sites, respectively, they are expected to be salted out at much higher NaBr concentrations; hence we do not see any additional peaks in these systems.

From these observations, it is clear that one set of peaks corresponds to lamellar periodicity, and the second set of peaks most probably coming from ordering within the plane of layers. In order to check this conjecture, we have analyzed diffraction data in detail and have found that these peaks could be indexed in a 2D rectangular lattice with lattice parameters ( $a=31.66 \text{ \AA}$ ,  $b=40.56 \text{ \AA}$ ). (**Table 2.5**). Similarly, ANT C12 showed similar salt induced ordering behavior as AFL C12.



**Figure 39: POM&X ray diffractograms of ANT-C12+ water system**

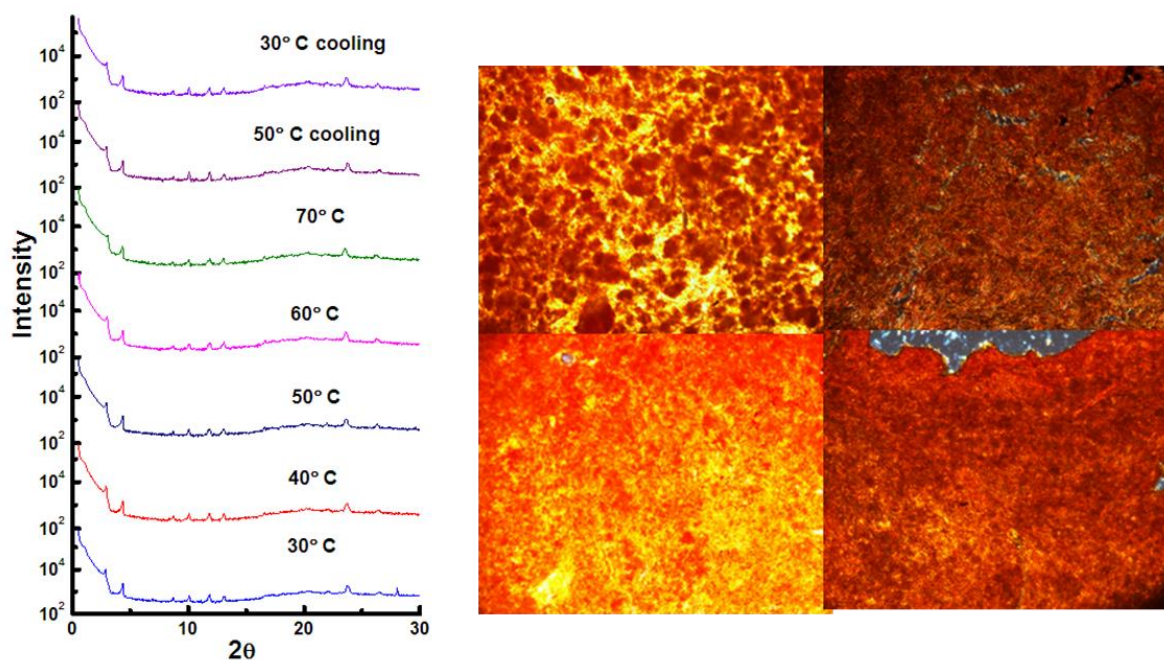


Figure 40: POM&X ray diffractograms of AFL-C12+ water system

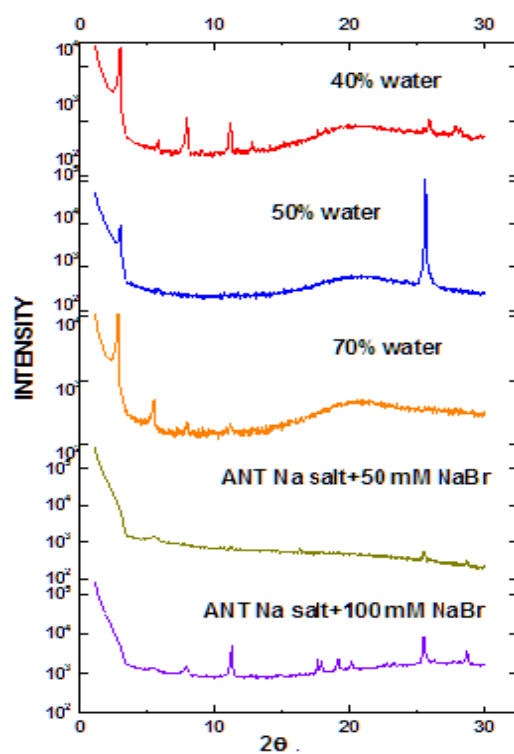
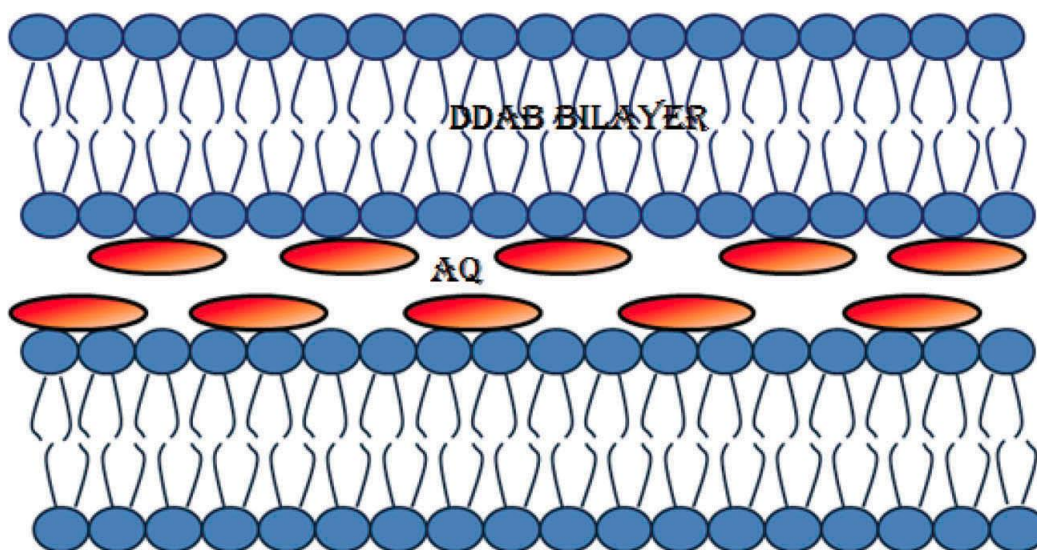


Figure 41: SAXS pattern of ANT sodium salt+ water +NaBr system

(h,k)	d <sub>calculated</sub> (Å)	d <sub>observed</sub> (Å)
(1,1)	24.32	24.96
(0,2)	20.28	20.28
(1,3)	12.37	12.43
(0,4)	10.14	10.13
(3,3)	8.32	8.73
(4,0)	7.91	7.44
(0,6)	6.76	6.73

**Table 2.5:** *d* spacings of AFL C12 complex +water (data is fitted into centered rectangular lattice with  $a=31.66\text{Å}$ ,  $b=40.56\text{Å}$ ) centered rectangular lattice as  $h+k$  is even)

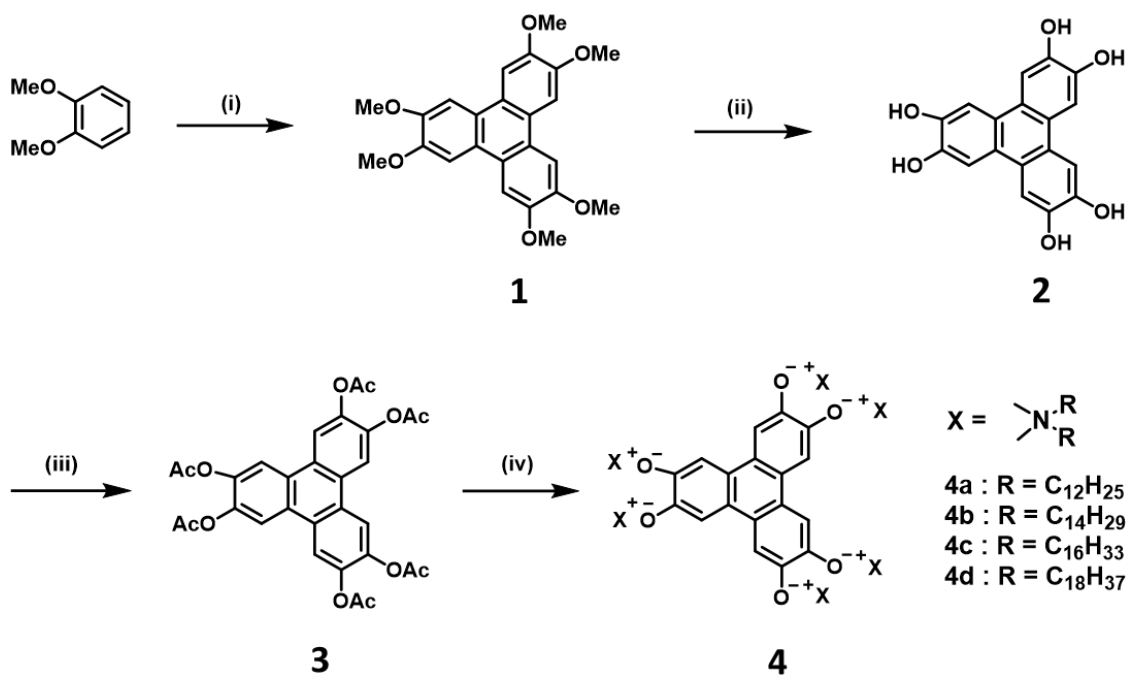
But in the case of AQ and AQ Octa sodium salt and DDAB system show  $L\alpha$  like SAXS pattern at different compositions. POM image shows the oily streaks which validates the lamellar pattern (Figure 42).



**Figure 42:** Proposed structure of AQ tectons-C12 + water system

### 2.3.2 Triphenylene-surfactant complexes:

Hexaacetoxo triphenylenes were prepared from hexamethoxytriphenylenes. Veratrole was trimerised using anhydrous  $\text{FeCl}_3$  to form hexamethoxy triphenylene. Further hexamethoxy triphenylene was deprotected using  $\text{HBr}/\text{AcOH}$  to form hexahydroxytriphenylenes. Further hexahydroxy triphenylene was esterified using acetic anhydride with drops of  $\text{H}_2\text{SO}_4$  as catalyst (as reported in literature). The products were confirmed using IR, NMR and elemental analysis. The ionic self-assembled complexes were synthesized via acetates.



**Scheme 1: Synthesis TP ISA complexes: (i)  $\text{FeCl}_3$ ; DCM,  $0^\circ\text{C}$  to RT 3 hrs; (ii)  $\text{HBr}/\text{AcOH}$  reflux 24hrs; (iii)  $\text{Ac}_2\text{O}$ ,  $\text{H}_2\text{SO}_4$  (catalytic), reflux overnight; (iv) 10M  $\text{NaOH}$ ,  $\text{R}_2\text{N}^+(\text{CH}_3)_2\text{Br}^-$  RT 24hrs ( $\text{R} = \text{C}_{12}\text{H}_{25}$ ,  $\text{C}_{14}\text{H}_{29}$ ,  $\text{C}_{16}\text{H}_{33}$ ;  $\text{C}_{18}\text{H}_{37}$ )**

The precipitate obtained from the reaction was soluble in organic solvents. The complexes were analyzed for the liquid crystalline behavior through microscopy, DSC and diffraction measurements. POM images show smectic textures.

The thermal stability of all the complexes was studied using TGA. TGA thermogram suggest that the complexes are thermally quite stable, the onset of decomposition was observed around 200 degrees ((**Figure 45**). The mesomorphic properties of complexes were studied using POM, DSC, and SAXS. POM images of complexes at different temperatures. POM images show textures typical of smectic phases. All of them show typical focal conic textures (**Figure 47**). Further, the mesomorphic behavior was confirmed through calorimetry studies. The DSC thermograms suggests that al the complexes show smectic transition apart from different crystal to crystal transitions. The enthalpy values show higher than typical values observed in the case of crystal to mesophase transition.

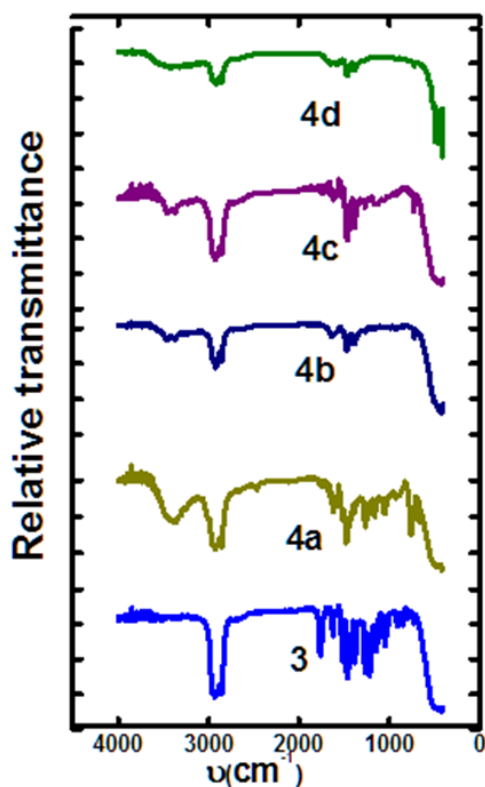


**Figure 43: IR spectra of 3 & 4 compounds (indicating absence of ester peaks in complexes)**

The DSC thermograms of the complexes are given in **Figure 46**. The temperature and corresponding enthalpy changes are given in table 1. The smectic nature of the mesophase was validated via x-ray diffraction studies.

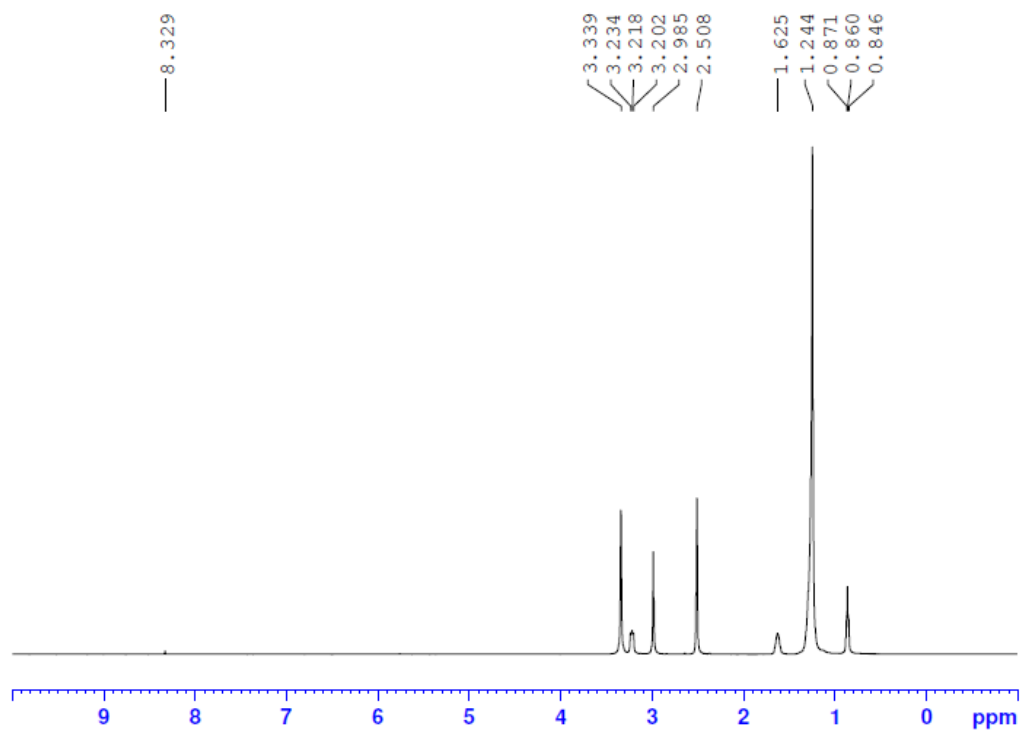


Figure 44: NMR of compound 4c

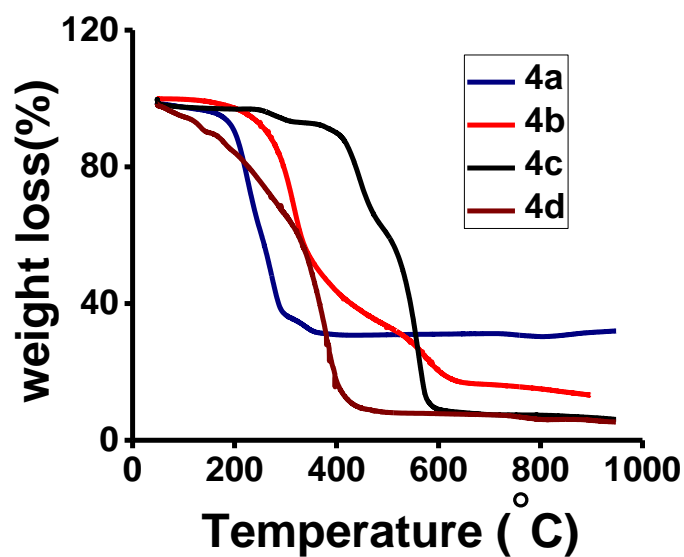


Figure 45: TGA profile of complexes 4a-d

The structural arrangement of complexes was analyzed via small-angle diffraction studies. The diffractograms of the complexes were recorded at appropriate temperatures. The diffractograms show peaks whose d spacing are in the ratio 1:1/2:1/3 (**Figure 48**) the wide-angle shows broad halo corresponding to the fluidity of alkyl chains. The d-spacings and corresponding indexation are given table 2.

### 2.3.2.1 Lyotropic behaviour:

The ionic self-assembled complexes were analyzed for lyotropic behavior in presence of water. The equimolar mixture of triphenylene polyelectrolyte (sodium salt) and surfactant was mixed with different amounts of water. The amount of polyelectrolyte and surfactant mixed was 1:6 ratio. After the equilibration of samples for 48 hours the samples were checked for mesomorphic behavior. Triphenylene hexa sodium salt with DDAB was complexed insitu and was hydrated with water. The 30% water system was analyzed using POM cryo-SEM and X-ray diffraction (**Figure 47**). The 30wt% water system was found to be lamellar as evidence from oily streaks from POM images and cryo-SEM images too validated lamellar arrangement. The diffraction patterns and POM textures were recorded until 80 degrees. The lamellar arrangement was retained until 80 degrees. 50wt% water and 70wt% water systems too showed lamellar phases which was further confirmed using cryo-SEM (**Figure 49-54**).

Comp	Weight (mg)	C	H	N	O	$n_s$	$n_c$	$n_s/n_c$
4a	4.6110	58.52	12.101	2.56	16.76	$8.42 \times 10^{-6}$	$1.196 \times 10^{-6}$	7.04
4b	2.188	66.60	12.281	2.30	18.61	$3.54 \times 10^{-6}$	$7.566 \times 10^{-7}$	4.75
4c	1.958	68.75	12.806	2.22	16.22	$3.10 \times 10^{-6}$	$3.8 \times 10^{-7}$	8.3
4d	1.2770	66.86	10.82	1.91	19.09	$1.735 \times 10^{-6}$	$2.90 \times 10^{-7}$	5.98

$n_s$ = number of moles of surfactants;  $n_c$ = number of moles of core

**Table 2.5: Elemental analysis of TP -surfactant complexes**

COMPOUND	Phase (temperature in °C)	d	Index
<b>4a</b>	<b>Smectic (120°C)</b>	27.31	10
		4.45	60
<b>4b</b>	<b>Smectic (95°C)</b>	31.37	10
		15.77	20
		4.49	70
<b>4c</b>	<b>Smectic (80°C)</b>	32.27	10
		16.16	20
		10.91	30
		4.53	70
<b>4d</b>	<b>Smectic (95°C)</b>	34.47	10
		17.20	20
		11.49	30
		4.26	80

**Table 2.6: d- spacings of TP -surfactant complexes**

The lower water composition systems were crystallites and non- mesomorphic. They showed phase segregation. 4d-70wt%water system was also mesomorphic. The lower water compositions exhibited phase segregation. Based on our diffraction observations we have proposed the electron density profile for the organization of the complexes in the presence of water. We have proposed possible electron density distribution that could possibly fit this current scenario (**Figure 55**). Based on observations we proposed a model for these complexes in the aqueous medium (**Figure 56**). Similar kind of arrangement was proposed for anthraquinone polyelectrolyte surfactant complex water systems<sup>42</sup>.

Table 2.7. <sup>a</sup> Phase transition temperatures (°C) and the corresponding energy changes (Jg<sup>-1</sup>)

Compd.	Phase sequence	
	Heating	Cooling
4a	Cr <sub>1</sub> 20.69 (46.82) Cr <sub>2</sub> 77.70(6.70) Sm 157.47 (2.26) I	I 153.86(--2.24)Sm
4b	Cr <sub>1</sub> 40.66 (51.40) Cr <sub>2</sub> 56.32(8.04) Sm 119.65 (4.82) I	I 107.98 (-5.55) Sm 53.12 (18.45)Cr
4c	Cr <sub>1</sub> 58.55(70.93)Cr <sub>2</sub> 78.58(24.76) Sm 155.41(4.01)I	I 136.16 (--5.83)Sm 54.63 (-22.40) Cr
4d	Cr 83.45 (67.88) Sm 143.69 ( 1.07) I	I 120.93(-2.01) Sm 62.15 (-9.58) Cr

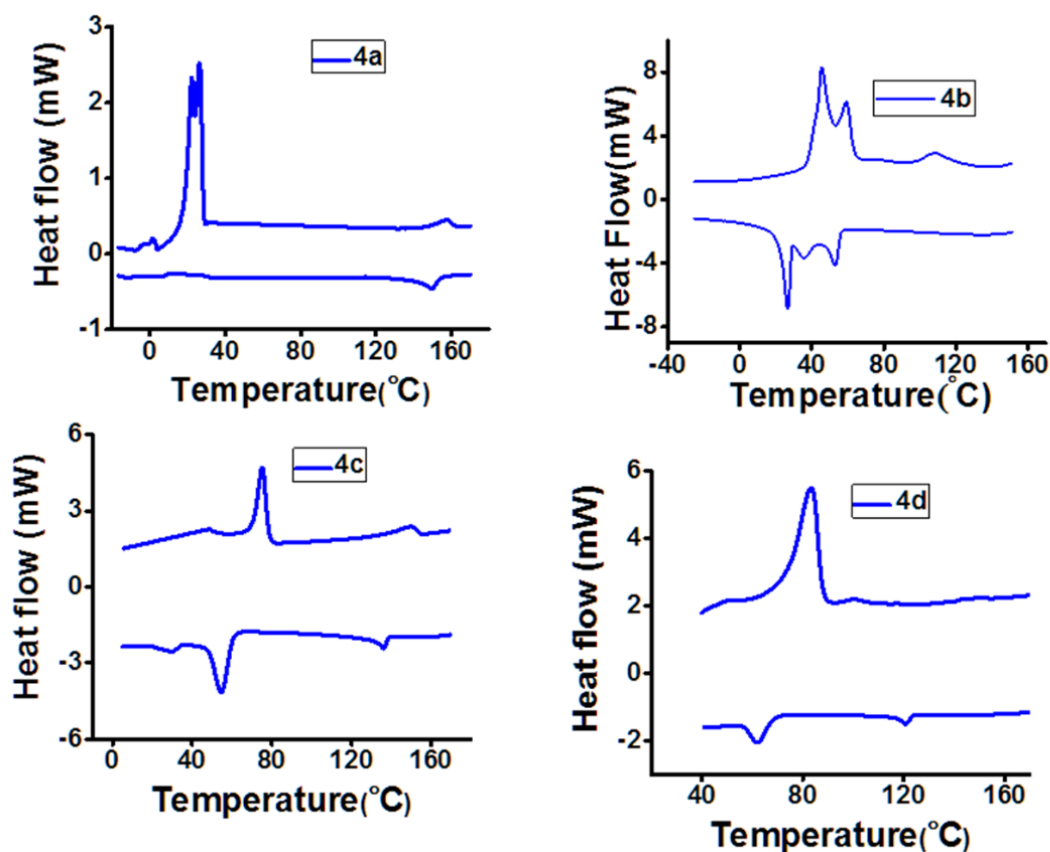


Figure 46: DSC thermograms of complexes

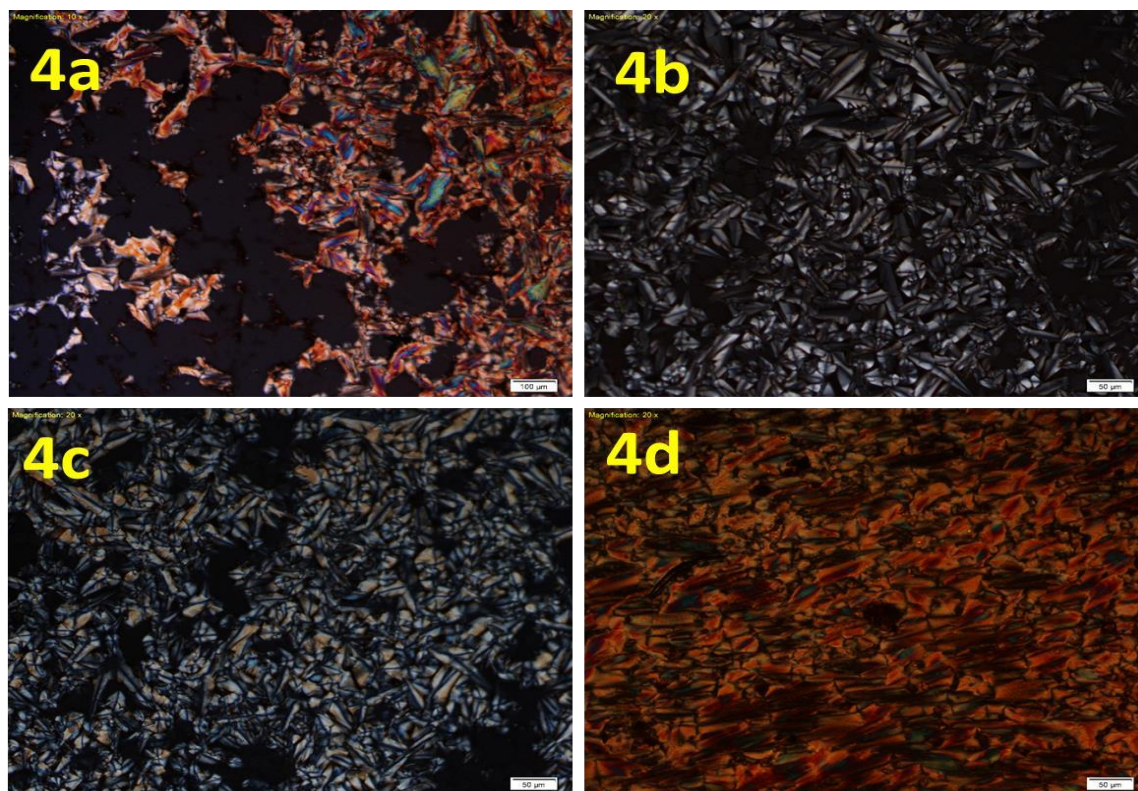


Figure 47: POM images of TP-IPA complexes: 4a at 95°C; 4b at 95 °C; 4c at 120°C; 4d at 90°C

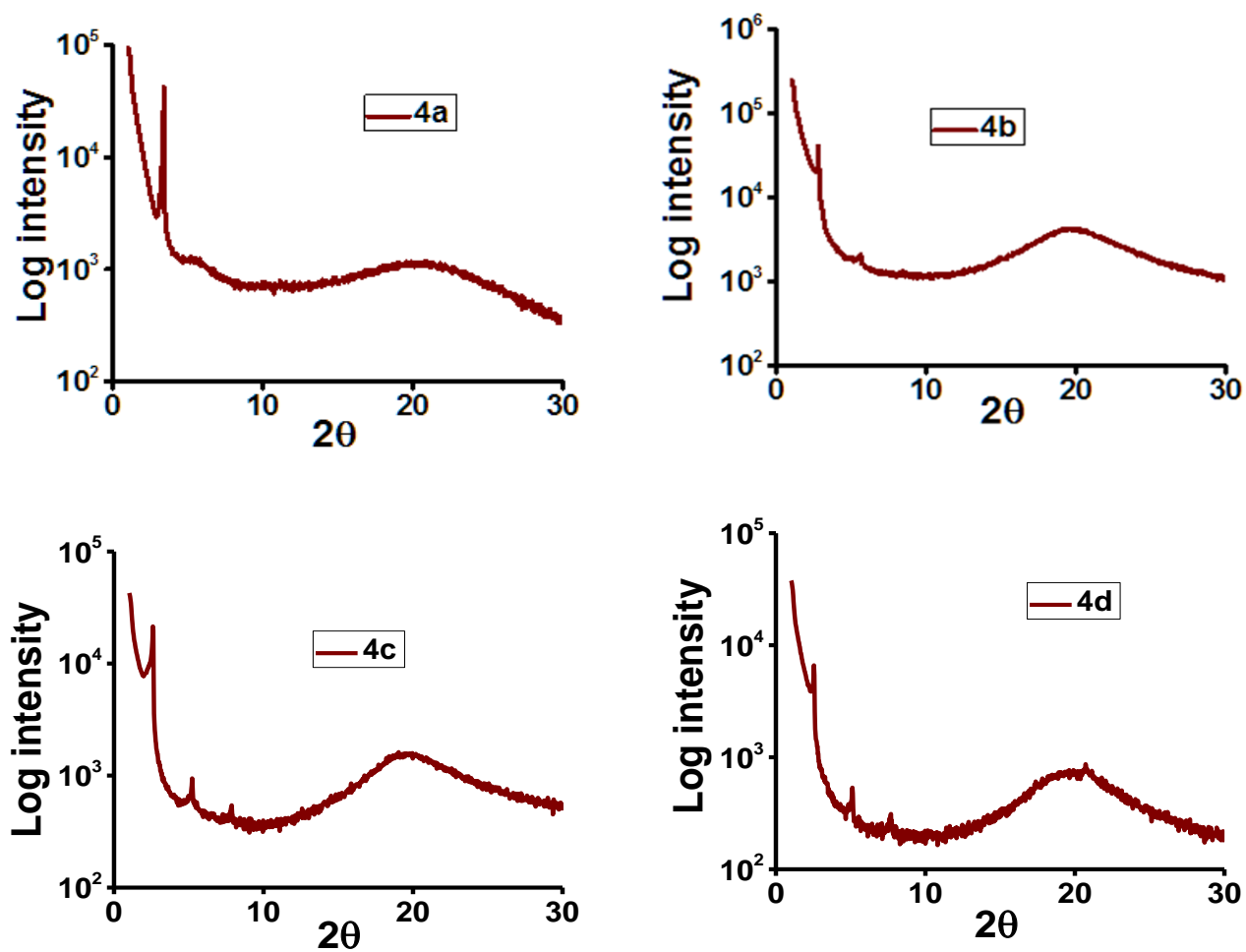


Figure 48: X-ray diffractograms of IPA complexes: 4a (95°C); 4b (90°C); 4c (120°C); 4d (90°C)

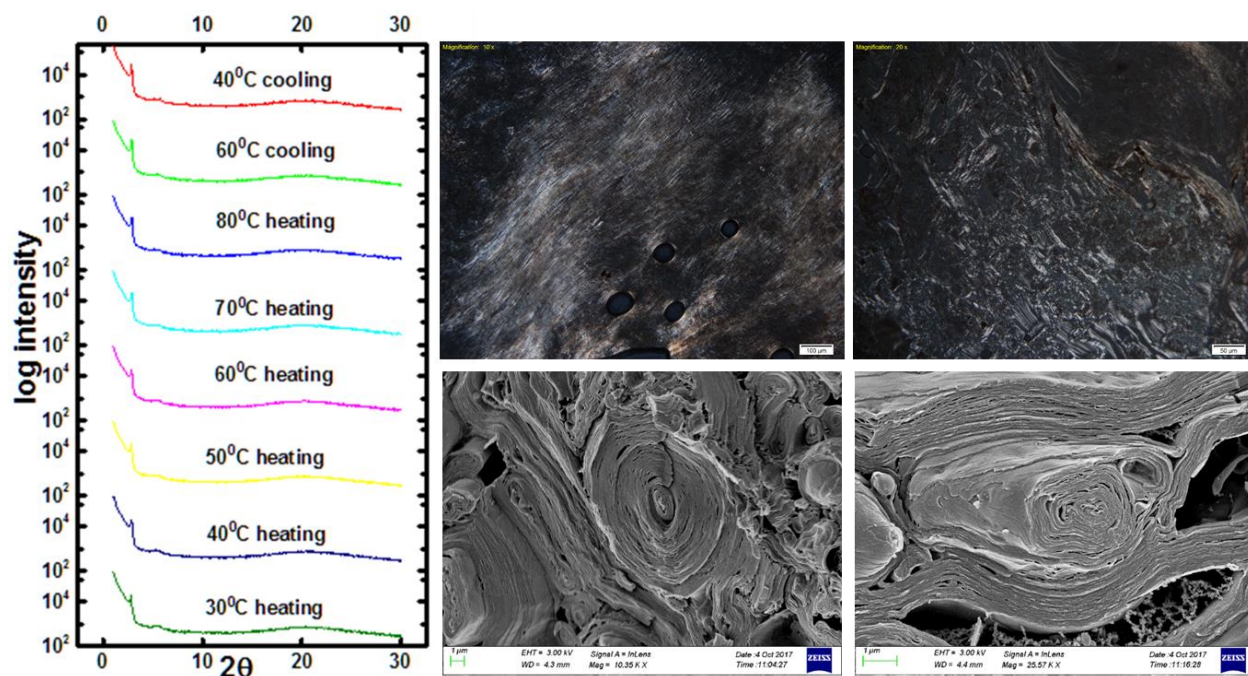


Figure 49: SAXS diffraction POM & Cryo SEM images of 4a-water (30 wt. %) system

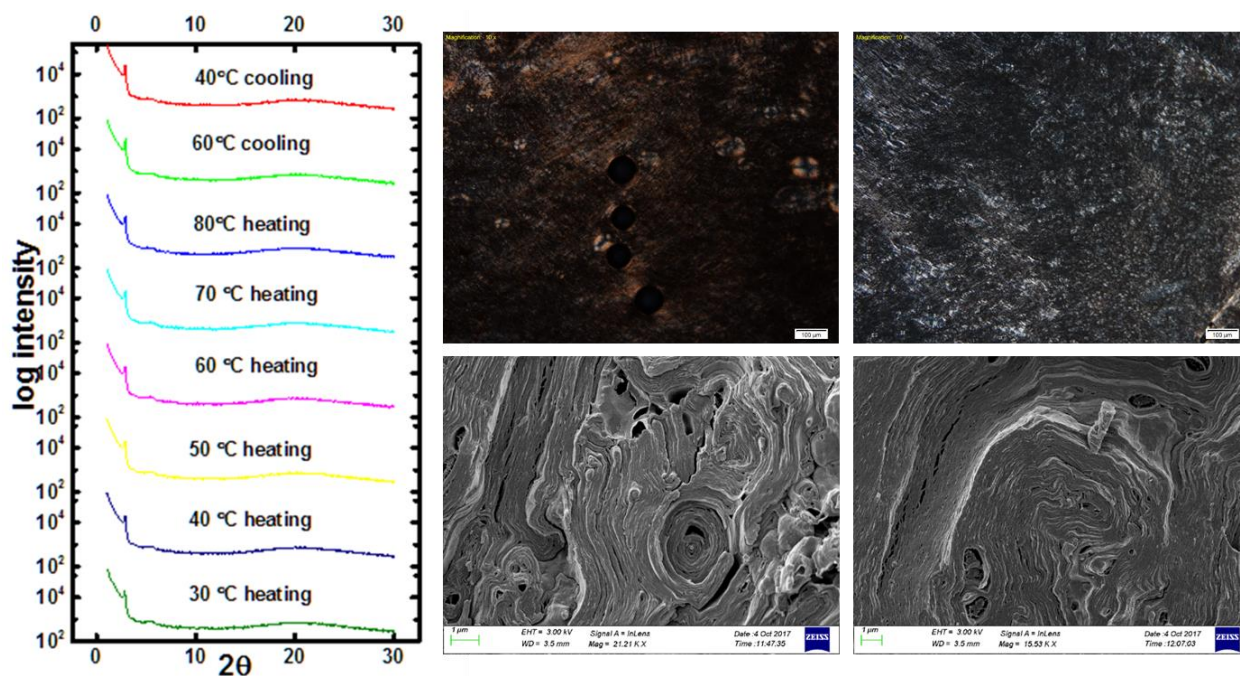


Figure 50: SAXS diffraction POM & Cryo SEM images of 4a-water (50 wt. %) system

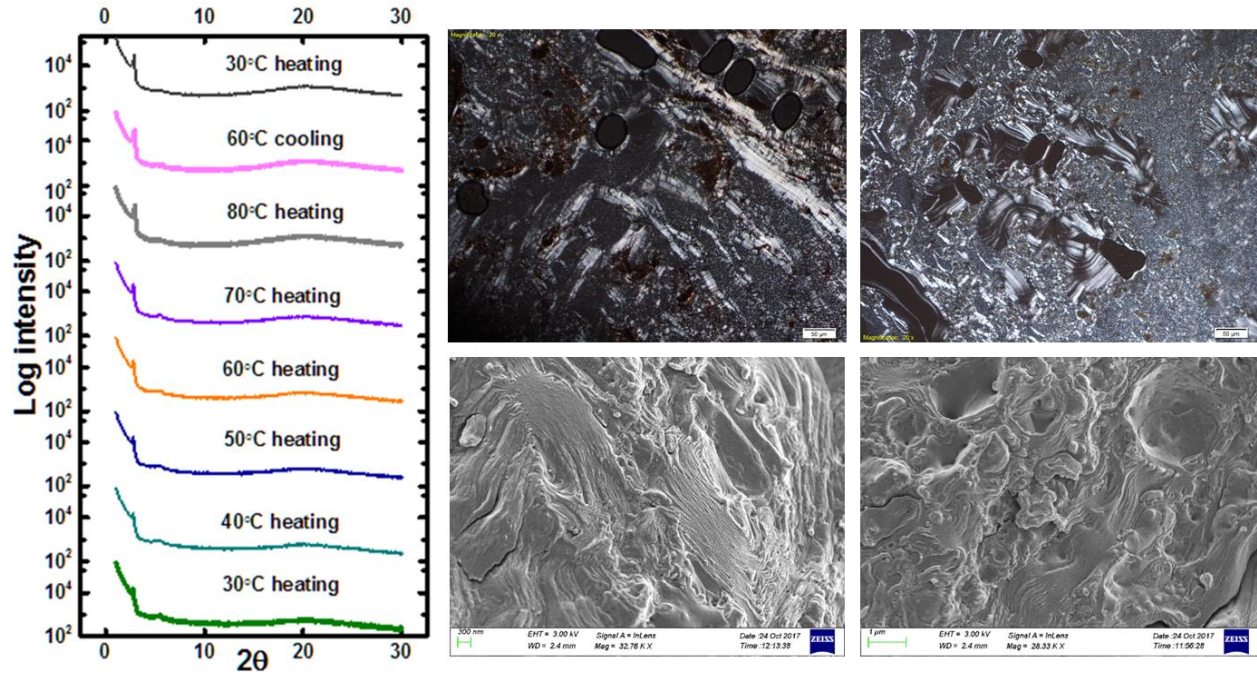


Figure 51: SAXS diffraction POM & Cryo SEM images of 4a-water (70 wt %) system

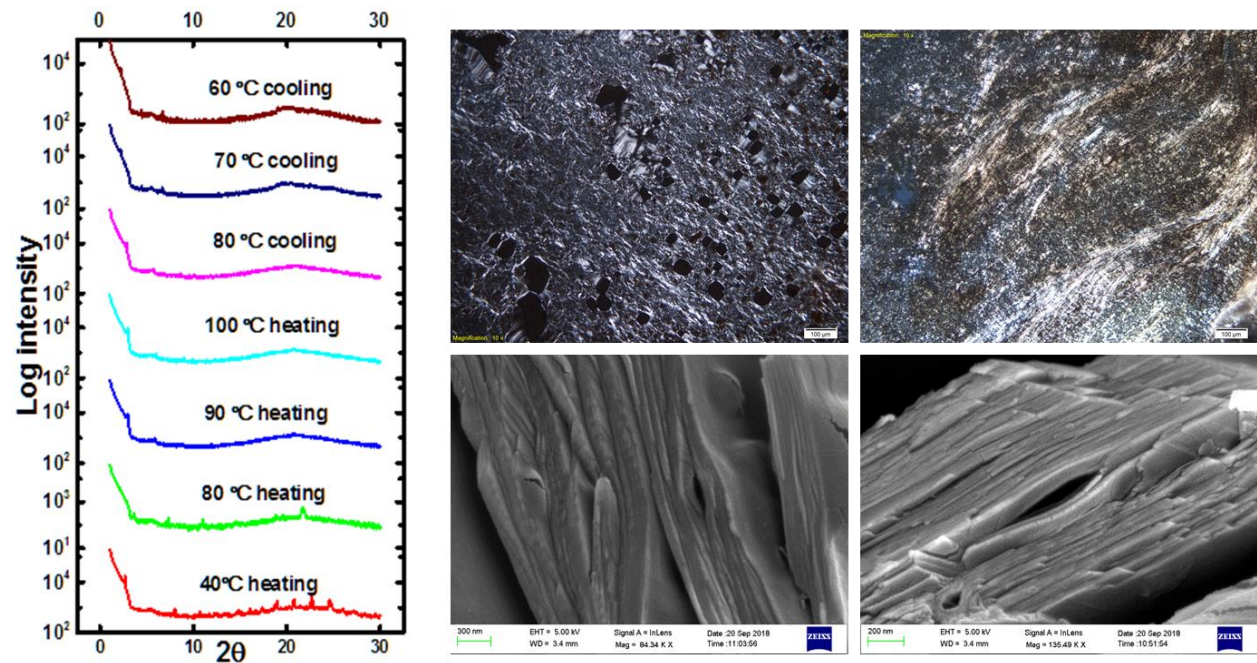


Figure 52: SAXS diffraction POM & Cryo SEM images of 4b-water (70 wt %) system

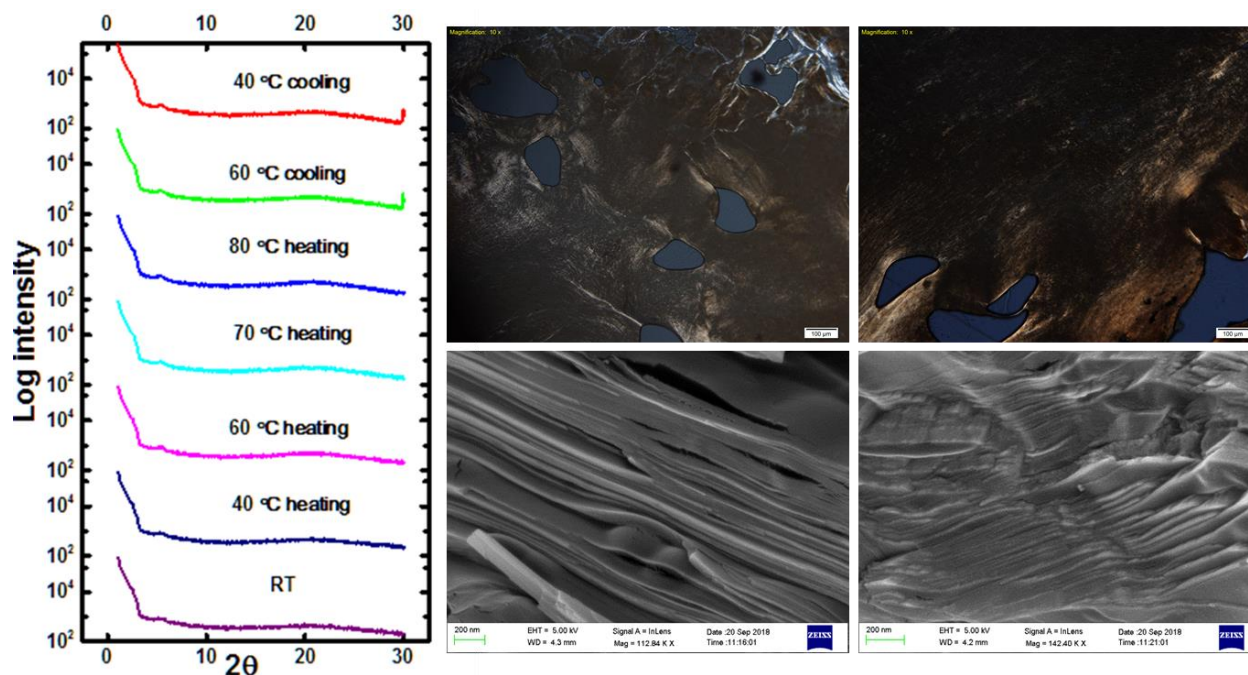


Figure 53: SAXS diffraction POM & Cryo SEM images of 4c-water (70 wt %) system

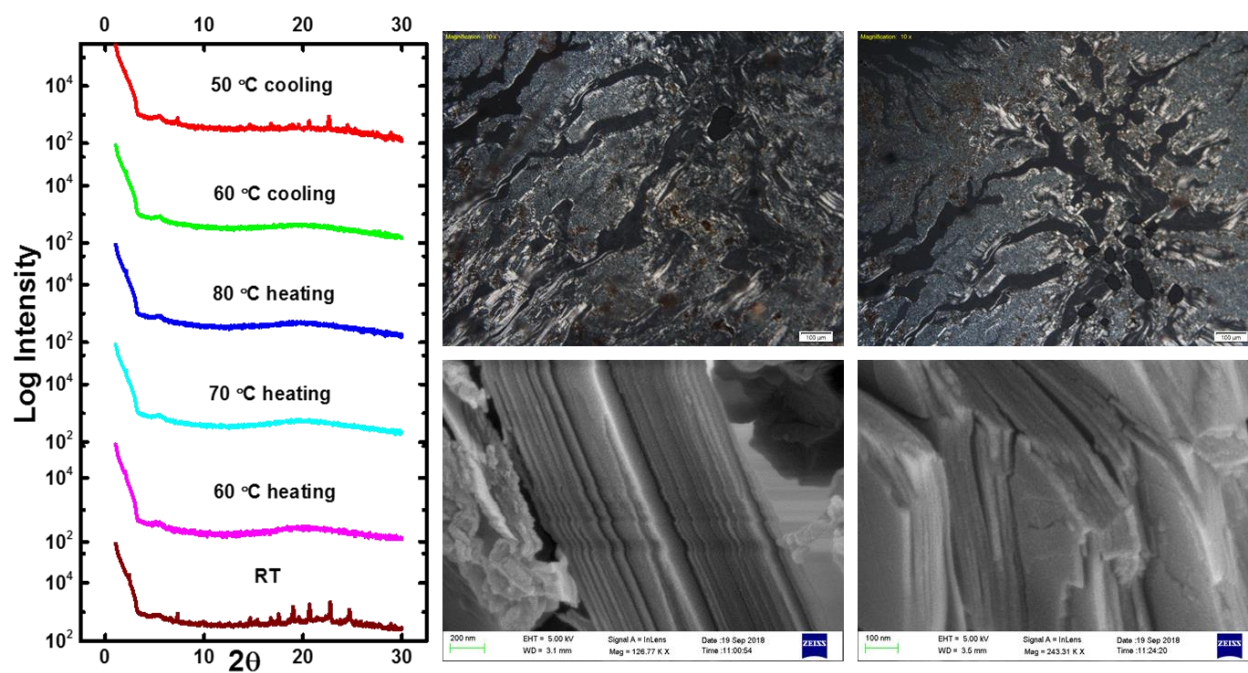


Figure 54: SAXS diffraction POM & Cryo SEM images of 4d-water (70 wt %) system

### 2.3.2.2 Analysis of X-ray diffraction pattern

X-ray diffraction pattern obtained as a function of scattering angle ( $\theta$ ) for "4a" is given in figure 49-51. Primary information obtained from the XRD pattern of the lamellar phase is d- spacing or lamellar repetitions and the intensity of peaks. For analysis of XRD data scattered intensity was plotted as the function of scattering vector  $q$  which is related to  $\theta$  by the following expression,

$$q = [4*\pi \text{ Sin } (\theta)]/\lambda$$

Where  $\lambda$  is the wavelength of x-ray used. From the intensity distribution of  $I(q)$  the electron density profile of the lamellar phase was constructed using the procedure detailed below.

In general, the diffraction pattern obtained from the sample contains scattering contribution from lattice as well as motif or basis- the individual scatterers spanning the lattice. These contributions can be expressed as,

$$I (q) = F (q)^2*S (q)$$

$S (q)$  is the structure factor that gives information about the lattice structure.  $F (q)$ , the form factor of the system, is related to scattering from the motif or basis.  $S (q)$  determines the position of the peaks and is a discrete function whereas  $F (q)$  gives the continuous intensity distribution of the diffraction pattern.

In the case of the lamellar phase, the structure factor is a set of delta functions at

$$q = h*q_0$$

Where  $q_0$  is related to lamellar d-spacing by the expression as follows,

$$q_0 = 2\pi / d$$

d - Lamellar periodicity and h= 1, 2, 3, etc. is the order of reflections.

Now the intensities obtained can be written as,

$$I(hq_0) = |F(hq_0)|^2$$

$|F(hq_0)|^2$  is the intensity at discrete positions defined by an integral multiple of  $q_0$ .  $|F(hq_0)|$  is the only direct readout from the pattern although  $F(hq_0)$  is, in general, a complex quantity.

The lamellar phase electron density profile along repeating direction Z can be represented by the Fourier series as given below,

$$\rho(z) = \sum_h (\alpha_h C_h F(hq_0) \cos(hq_0 z))$$

Where  $\alpha_h$  defines the unknown phase corresponding to  $F(hq_0)$ . For a centrosymmetric motif,  $\alpha_h$  takes the value +1 or -1, which reduces the possible combination of phases to  $2^n$  for n number of reflections.  $C_h$  is the scaling factor accounting for the scattering geometry and the sample morphology. Normalizing the intensities of higher-order peaks with respect to the h=1 peak takes care of this unknown scaling factor. The electron density in this relative scale reads as,

$$\rho(z)_{rel} = \sum_h (\alpha R_h \cos(hq_0 z))$$

Where  $R_h = |F(hq_0)| / |F(q_0)|$

The electron density profile obtained for 4(b) are shown in Figure 55. Combinations of phases (- + -) were chosen as reasonably correct from all 8 possible phase combinations obtained by the intensity analysis done for 3 peaks.

In **figure 55** the minima show the center of bilayer with hydrophilic groups surrounding on either side validates our observations. This made us to propose the following model (**Figure 56**) for the organization of these complexes

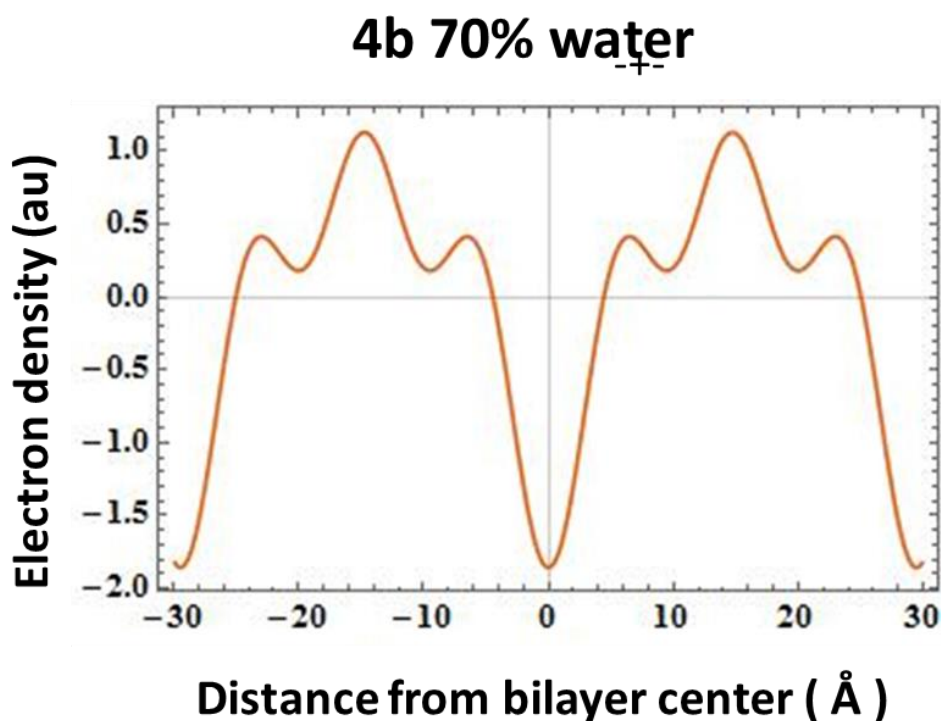


Figure55: Electron density profile for (-+-) combination for 4b-water (70 wt %) system

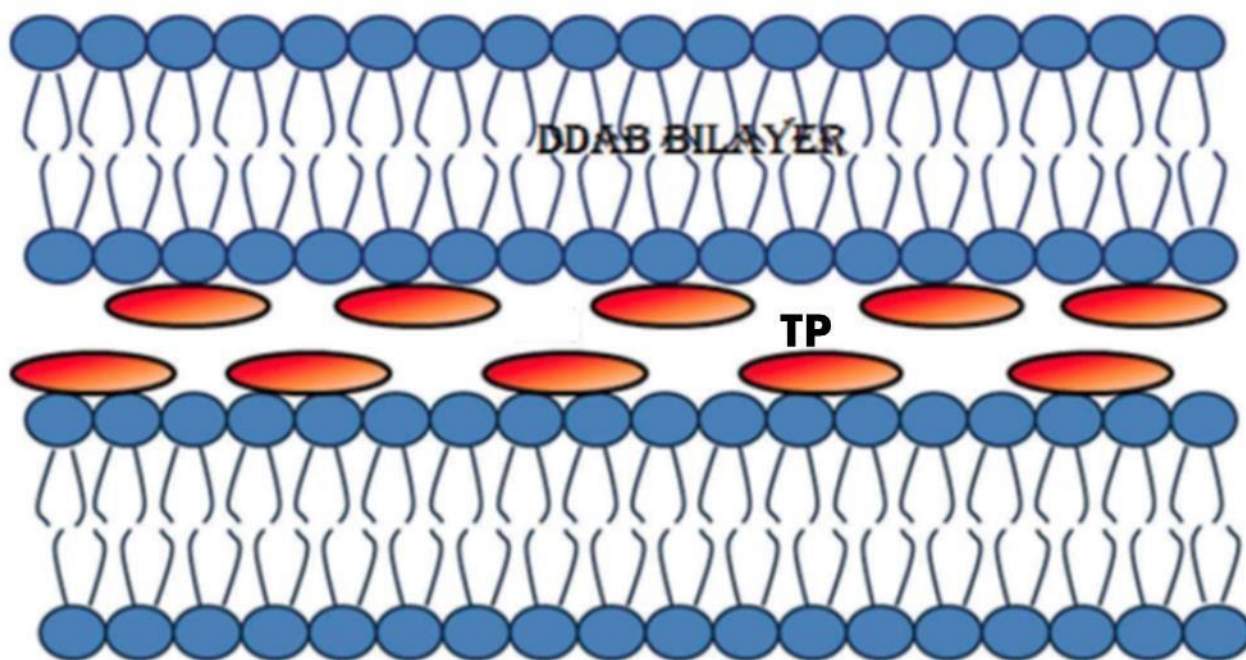


Figure56: Proposed model for triphenylene-surfactant –water system

## 2.4 Conclusion

This chapter describes the preparation of ionic self-assembled complexes and their mesomorphic behaviour. The chapter involves two parts one involves anthraquinones as tecton whereas the other involve triphenylene tecton. The triphenylenes and anthraquinones have been one of the widely explored discotic systems where they usually found to be exhibiting columnar behavior. Here we tried inducing the mesophase behavior in the core itself with double tail surfactants binds them via ionic self-assembly approach.

## 2.5 Experimental Section

### General Methods:

The chemical structures of the compounds were determined using a combination of spectroscopic techniques. Infrared spectra were recorded using a Shimadzu FTIR–8400 spectrophotometer. <sup>1</sup>H NMR spectra were recorded on a Bruker AMX 400 spectrometer using tetramethylsilane (TMS) as an internal standard. The elemental analysis was carried out for all the intermediate and final compounds using a Carlo-Erba 1106 elemental analyzer. A Perkin-Elmer, Pyris 1 differential scanning calorimeter (DSC) was used to determine the transition temperature and the associated enthalpy values for all the mesogenic compounds. In all cases, heating and cooling rates were 5 °C/min. The mesophase textures were observed using an Olympus BX50 polarizing optical microscope equipped with a Mettler FP82HT heating stage and a Mettler FP90 central processor.

X-ray diffraction (XRD) measurements on powder samples were carried out using PANalytical, Empyrean diffractometer using Cu-K<sub>α</sub> ( $\lambda = 1.54 \text{ \AA}$ ) beam. The sample was held in Lindemann capillaries (0.7mm diameter)

### Synthesis:

#### **Synthesis of Rufigallol:**

Rufigallol is prepared following the reported procedure <sup>43</sup>. A mixture of Gallic acid (10 g) and conc. H<sub>2</sub>SO<sub>4</sub> (40 ml) was heated with stirring at 100 °C for 3h. The reaction mixture was cooled and poured over crushed ice and the orange precipitate obtained was filtered and washed with cold water, dried under vacuum to get crude rufigallol as a brown solid (4 g, 49 %). The crude rufigallol was used in the subsequent steps without any further purification.

#### **Synthesis of ANT acetate, AFL Acetate:**

The solution of anthraflavic acid and anthrarufin in dichloromethane was cooled to 0°C. To the cooled solution, acetyl chloride solution was added. The mixture was stirred at room temperature overnight. The mixture was poured into water and washed with water a few times. The resultant organic layer was evaporated and recrystallized from methanol. The obtained material was used as such for further steps.

### **Synthesis of AQ acetate & AQ Octa acetate:**

Rufigallol /octa hydroxy anthraquinone (1g) was dissolved in acetic anhydride and drops of H<sub>2</sub>SO<sub>4</sub> was added. The resultant mixture was refluxed overnight. The hot solution was poured into ice. The precipitate obtained was filtered and washed till the washing are neutral. The precipitate was dried in a vacuum and used for further steps.

### **Synthesis of hexamethoxy triphenylene:**

To a suspension of FeCl<sub>3</sub> (36.96 g, 227.85 mmol, 9.3 equiv) in CH<sub>2</sub>Cl<sub>2</sub> (200 mL) and H<sub>2</sub>SO<sub>4</sub> (0.5 mL), was added dropwise a solution of veratrole (9.4 mL, 73.5 mmol, 3 equiv) in CH<sub>2</sub>Cl<sub>2</sub> (100 mL). The reaction mixture was stirred at room temperature for 3 h and quenched by slow addition of methanol (300 mL) at 0 °C. The mixture was further stirred for 0.5 h and the obtained precipitate was filtered, washed with methanol, and dried in vacuum. The grey solid (7.75 g, 78 %) was used in the next step without further purification

### **Synthesis of hexahydroxy triphenylene:**

A solution of **1** (3.00 g, 7.2 mmol, 1 equiv) in a mixture of glacial CH<sub>3</sub>COOH (100 mL) and 48 wt% aqueous HBr (100 mL) was bubbled with argon for 0.5 h. The grey suspension was stirred at reflux under argon for 12 h. The mixture was cooled down to room temperature and then filtered, washed with cold water and dried. The grey solid was recrystallized from CH<sub>3</sub>COOH/H<sub>2</sub>O (3:2, 200 mL) by treating with activated carbon, affording gray crystals (1.12 g, 48 %), which were stored under argon.

### **Synthesis of triphenylene hexaacetate:**

The solution of hexahydroxy triphenylene (2g) in acetic anhydride (50ml) and 5 drops of H<sub>2</sub>SO<sub>4</sub> was refluxed overnight. The hot solution was poured in ice and the precipitate was filtered under vacuum. The precipitate was washed with a large amount of water until the washings were neutral and dried. The dried precipitate was dissolved in chloroform and reprecipitated using methanol which was used for further reaction

**General procedure for preparation of ISA complexes:**

The AQ or TP acetate (1eq) was dispersed in 10N NaOH solution. The dispersion was stirred for 15 minutes. The solution of surfactant (appropriate equivalents as per no of acetates in the core) in 10N NaOH solution was added to the above prepared solution. The mixture was stirred for 48 hrs at room temperature. After 48hrs there was precipitate floating in the medium. The mixture was centrifuged in order to remove the precipitate (as they were sticky cannot be filtered through filter paper). The precipitate collected after centrifugation was subjected to water washing multiple times in order to remove the excess base present in the precipitate. The obtained precipitate was dried under high vacuum. The powder was used for further characterization.

## 2.6 References and Notes

1. Steed, J. W., Atwood, J. L. & Gale, P. A. Definition and Emergence of Supramolecular Chemistry. in *Supramolecular Chemistry: From Molecules to Nanomaterials* (2012). doi:10.1002/9780470661345.smc002
2. Hobza, P. & Müller-Dethlefs, K. Non-covalent interactions: Theory and experiment. *RSC Theor. Comput. Chem. Ser.* (2009).
3. Bruce, D. W. Liquid Crystals Formed from Specific Supramolecular Interactions. in *Supramolecular Chemistry* (John Wiley & Sons, Ltd, 2012). doi:10.1002/9780470661345.smc149
4. Steed, J. . & Atwood, J. L. *1- Concepts. Supramolecular Chemistry* (2000). doi:10.1002/9780470740880
5. Faul, C. F. J. & Antonietti, M. Ionic Self-Assembly: Facile Synthesis of Supramolecular Materials. *Adv. Mater.* **15**, 673–683 (2003).
6. Faul, C. F. J. Ionic Self-Assembly for Functional Hierarchical Nanostructured Materials. *Acc. Chem. Res.* **47**, 3428–3438 (2014).
7. *Supramolecular Soft Matter. Supramolecular Soft Matter* (John Wiley & Sons, Inc., 2011). doi:10.1002/9781118095331
8. Holman, K. T., Pivovar, A. M., Swift, J. A. & Ward, M. D. Metric Engineering of Soft Molecular Host Frameworks. *Acc. Chem. Res.* **34**, 107–118 (2001).
9. MacLachlan, M. J. *et al.* Mesostructured Metal Germanium Sulfides. *J. Am. Chem. Soc.* **121**, 12005–12017 (1999).
10. Zhang, T., Brown, J., Oakley, R. J. & Faul, C. F. J. Towards functional nanostructures: Ionic self-assembly of polyoxometalates and surfactants. *Curr. Opin. Colloid Interface Sci.* **14**, 62–70 (2009).
11. Zhou, S. & Chu, B. Assembled Materials: Polyelectrolyte-Surfactant Complexes. *Adv. Mater.* **12**, 545–556 (2000).

12. Ozer, B. H., Smarsly, B., Antonietti, M. & Faul, C. F. J. DNA-analogous structures from deoxynucleophosphates and polylysine by ionic self-assembly. *Soft Matter* **2**, 329 (2006).
13. Thünemann, A. F. Polyelectrolyte-surfactant complexes (synthesis, structure and materials aspects). *Progress in Polymer Science (Oxford)* (2002). doi:10.1016/S0079-6700(02)00017-5
14. Rembaum, A. Polyelectrolyte Complexes. *J. Macromol. Sci. Part A - Chem.* **3**, 87–99 (1969).
15. El-Shishtawy, R. M. Functional Dyes, and Some Hi-Tech Applications. *Int. J. Photoenergy* **2009**, 1–21 (2009).
16. Faul, C. F. J. & Antonietti, M. Facile Synthesis of Optically Functional, Highly Organized Nanostructures: Dye–Surfactant Complexes. *Chem. - A Eur. J.* **8**, 2764 (2002).
17. Zhao, M., Zhao, Y., Zheng, L. & Dai, C. Construction of Supramolecular Self-Assembled Microfibers with Fluorescent Properties through a Modified Ionic Self-Assembly (ISA) Strategy. *Chem. - A Eur. J.* **19**, 1076–1081 (2013).
18. Zakrevskyy, Y., Stumpe, J. & Faul, C. F. J. A Supramolecular Approach to Optically Anisotropic Materials: Photosensitive Ionic Self-Assembly Complexes. *Adv. Mater.* **18**, 2133–2136 (2006).
19. Guan, Y., Yu, S.-H., Antonietti, M., Böttcher, C. & Faul, C. F. J. Synthesis of Supramolecular Polymers by Ionic Self-Assembly of Oppositely Charged Dyes. *Chem. - A Eur. J.* **11**, 1305–1311 (2005).
20. Dutta, R., Pyne, A., Kundu, S., Banerjee, P. & Sarkar, N. Concentration-Driven Fascinating Vesicle-Fibril Transition Employing Merocyanine 540 and 1-Octyl-3-methylimidazolium Chloride. *Langmuir* **33**, 9811–9821 (2017).
21. Kumar, S. Self-organization of disc-like molecules: chemical aspects. *Chem. Soc. Rev.* **35**, 83–109 (2006).
22. Thünemann, A. F., Ruppelt, D., Burger, C. & Müllen, K. Long-range ordered columns of

- a hexabenzob[bc,ef,hi,kl,no,qr]coronene–polysiloxane complex: towards molecular nanowires. *J. Mater. Chem.* **10**, 1325–1329 (2000).
23. Thünemann, A. F., Ruppelt, D., Ito, S. & Müllen, K. Supramolecular architecture of a functionalized hexabenzocoronene and its complex with polyethyleneimine. *J. Mater. Chem.* **9**, 1055–1057 (1999).
24. Guan, Y., Zakrevskyy, Y., Stumpe, J., Antonietti, M. & Faul, C. F. J. Perylenediimide-surfactant complexes: thermotropic liquid-crystalline materials via ionic self-assembly. Electronic supplementary information (ESI) available: <sup>1</sup>H-NMR, IR, UV and fluorescence spectra of 1. See <http://www.rsc.org/suppdata/cc/b2/b211753c/>. *Chem. Commun.* 894–895 (2003). doi:10.1039/b211753c
25. Zakrevskyy, Y., Faul, C. F. J., Guan, Y. & Stumpe, J. Alignment of a Perylene-Based Ionic Self-Assembly Complex in Thermotropic and Lyotropic Liquid-Crystalline Phases. *Adv. Funct. Mater.* **14**, 835–841 (2004).
26. Kadam, J., Faul, C. F. J. & Scherf, U. Induced Liquid Crystallinity in Switchable Side-Chain Discotic Molecules. *Chem. Mater.* **16**, 3867–3871 (2004).
27. Camerel, F. & Faul, C. F. J. Combination of ionic self-assembly and hydrogen bonding as a tool for the synthesis of liquid-crystalline materials and organogelators from a simple building block. Electronic supplementary information (ESI) available: IR, NMR, DSC and TGA data of the organ. *Chem. Commun.* 1958 (2003). doi:10.1039/b303552b
28. Zakrevskyy, Y., Smarsly, B., Stumpe, J. & Faul, C. F. J. Highly ordered monodomain ionic self-assembled liquid-crystalline materials. *Phys. Rev. E* **71**, 021701 (2005).
29. Franke, D., Vos, M., Antonietti, M., Sommerdijk, N. A. J. M. & Faul, C. F. J. Induced Supramolecular Chirality in Nanostructured Materials: Ionic Self-Assembly of Perylene-Chiral Surfactant Complexes. *Chem. Mater.* **18**, 1839–1847 (2006).
30. Camerel, F., Ulrich, G., Barberá, J. & Ziessel, R. Ionic Self-Assembly of Ammonium-Based Amphiphiles and Negatively Charged Bodipy and Porphyrin Luminophores. *Chem. - A Eur. J.* **13**, 2189–2200 (2007).

31. Ma, T., Li, C. & Shi, G. Optically Active Supramolecular Complex Formed by Ionic Self-Assembly of Cationic Perylenediimide Derivative and Adenosine Triphosphate. *Langmuir* **24**, 43–48 (2008).
32. Hu, J. *et al.* Self-Assembled Sugar-Substituted Perylene Diimide Nanostructures with Homochirality and High Gas Sensitivity. *Adv. Funct. Mater.* **22**, 4149–4158 (2012).
33. Lu, L. *et al.* Ionic Self-Assembled Derivative of Tetraphenylethylene: Synthesis, Enhanced Solid-State Emission, Liquid-Crystalline Structure, and Cu<sup>2+</sup> Detection Ability. *ChemPhysChem* **18**, 3605–3613 (2017).
34. Cui, K. *et al.* Reversible Anion-Driven Switching of an Organic 2D Crystal at a Solid-Liquid Interface. *Small* **13**, 1702379 (2017).
35. Huang, Y. *et al.* Highly responsive ethylenediamine vapor sensor based on a perylenediimide–camphorsulfonic acid complex via ionic self-assembly. *J. Mater. Chem. C* **5**, 7644–7651 (2017).
36. Eisermann, J., Prager, L. & Hinderberger, D. Solvent and concentration effects on highly defined, colloid-like ionic clusters in solution. *Phys. Chem. Chem. Phys.* **20**, 1421–1430 (2018).
37. Zhao, Y., Zhang, L., Zhang, Y. & Yang, W. Fabrication of fluorescent star-like supramolecular materials through a novel ionic self-assembly strategy. *J. Mol. Liq.* **250**, 369–374 (2018).
38. Knelles, J. *et al.* Self-Assembly and Fluorescence of Tetracationic Liquid Crystalline Tetraphenylethene. *ChemPhysChem* **20**, 2210–2216 (2019).
39. Xie, Y. *et al.* Interwoven Molecular Chains Obtained by Ionic Self-Assembly of Two Iron(III) Porphyrins with Opposite and Mismatched Charges. *ACS Appl. Mater. Interfaces* **11**, 34203–34211 (2019).
40. Zhong, Y., Wang, J. & Tian, Y. Binary ionic porphyrin self-assembly: Structures, and electronic and light-harvesting properties. *MRS Bull.* **44**, 183–188 (2019).

41. Tan, C. & Wang, Y. Ionic self-assembly of organic-polyxometalate hybrids in solid state and its charge transfer properties. *J. Solid State Chem.* **277**, 381–387 (2019).
42. Swamynathan, K., Raghunathan, V. A. & Kumar, S. Synthesis and mesomorphism of ionic self-assembled complexes of anthraquinones. *Liq. Cryst.* **44**, 2311–2320 (2017).
43. Grimshaw, J. & Haworth, R. D. 813. Flavogallol. *J. Chem. Soc.* 4225 (1956).  
doi:10.1039/jr9560004225